Automated Cutter Size and Orientation Determinations for Multi-Axis Sculptured Part Milling

GANG LIU

A Thesis

in

the Department

of

Mechanical & Industrial Engineering

Presented in Partial Fulfillment of the Requirements

for the Degree of Master of Applied Science (Mechanical Engineering) at

Concordia University

Montreal, Quebec, Canada

March 2007

Your file Votre référence
ISBN: 978-0-494-34706-5
Our file Notre référence
ISBN: 978-0-494-34706-5

Abstract

Automated Cutter Size and Orientation Determinations for Multi-Axis Sculptured Part Milling

Gang Liu

In CNC machining of sculptured surface parts, using larger cutters can get better surface quality and higher productivity. However, the chance of gouging and interfering with the part surfaces during machining increases. In my thesis research, an innovative, generic method is proposed to determine optimal cutter sizes and orientations for 3- and 4-axis free-form surface end-milling without gouging and interference. The main research contribution is that, to cut a part surface at a cutter-contact point, the size and orientation of the optimal cutter, which is the minimum of all imaginary cutters that over-cut or collide with the part surfaces, are formulated with a global optimization problem. My work has proposed a hybrid global optimization method, which is a combination of the particle swarm optimization method and the local optimization method, and applied it to this optimization problem. Thus, the calculated optimal cutter is the largest tool to machine the cutter-contact point without gouging and interference. Based on the optimal cutters for all the cutter-contact points, a group of standard end-mills can be selected to be as large as possible for machining these part surfaces. To demonstrate the advantages of this new approach, two sculptured parts are adopted, one is a hair dryer mold with 24 free-form surface patches and the other is an axial-flow compressor. By applying this approach, a group of cutters and their orientations can be determined to achieve a high machining efficiency and ensure the surface accuracy and finish. The 3- and 4-axis machining for these parts are simulated with the CATIA V5 CAD/CAM system.

Acknowledgements

I would like to thank my supervisor, Dr. Zezhong C. Chen, for his guidance and support for this research topic. I really appreciate his enthusiasm, encourage, expertise, and research philosophy. To Qiang Fu, Hong Da Zhang, Saeed Al-Taher, Shahid Khan, Tian Bo Zhao, Guo Gui Huang, and Hong Zheng, I give my thanks for their encouragement, their valuable insight, and their comments.

On a personal side, my wonderful wife Qi Hong deserves the most thanks, for her patience, consistent support, and consideration. To my son Yu Qing, I love him very much.

Table of Contents

List of Figures

List of Tables

Chapter 1 Introduction

1.1 CNC machining

1.1.1 Definition of computerized numerical control (CNC)

CNC is the abbreviation of Computerized Numerical Control. It is developed from the NC (Numerical Control) technology which was invented by John T. Parsons in collaboration with MIT Servomechanisms Laboratory. NC uses a fixed logical functions which are built-in and permanently wired in the control unit. These functions cannot be modified by programmers or machinists. So, an NC system can interpret NC programs but does not allow any changes to them. A CNC system stores a variety of routines in an internal micro-processor and memory to manipulate logical functions. This gives flexibility for programmers or machine operators to change the program in the control. It is the greatest advantage of CNC systems compared to NC systems.

1.1.2 Conventional and CNC machining

Conventional and CNC machining processes are the same in the following approaches to machining parts:

- Obtain and study part drawings
- Select the most suitable machining method
- Decide on the setup method (work holding)
- Select cutting tools
- Establish speeds and feeds
- Machine the part

In conventional machining, the machinist manually sets up a workpiece on the machine and operates a cutting tool to remove the stock material. Thus, the produced parts in a batch are often inconsistent. Consequently, maintaining the required dimensional tolerances and surface finish quality is the most typical problem in conventional machining. Fortunately, the machining under numerical control can get rid of this problem. Once the NC program for machining a part has been verified, it can be used over and over again to generate quality-consistent products. In production planning for a batch of parts, the batch size usually determines whether using CNC machining or conventional machining; more importantly, the part complexity, tolerances, and surface finish should be taken into account.

1.1.3 Advantages of CNC machining

CNC machining demonstrates its advantages compared with conventional machining in the following areas:

- Setup time reduction
- Lead time reduction
- Accuracy and repeatability
- Contouring of complex shapes
- Simplified tooling and work holding
- Consistent cutting time
- General productivity increase

1.1.4 Types of CNC machines

In industry, there are many types of CNC machine tools, and some of the commonly used are listed as:

- Milling and machining centers
- Laths and turning centers
- Drilling machines
- Boring mills and profilers
- EDM machines

- Punch presses and shears
- Flame cutting machines
- Routers
- Water jet and Laser profilers
- Cylindrical grinders
- Welding machines
- Benders, winding and spinning machines, etc.

Among all these machine tools, multi-axis CNC milling machines and lathes dominate the number of installations in the manufacturing industry. For example, 3- and 5-axis CNC milling machines and 2- and 3-axis CNC turning machines. Regarding to a 3-axis CNC milling machine, the cutter can move simultaneously along X, Y and Z axes. A 5-axis CNC milling machine can simultaneously execute cutter motions not only along X, Y and Z axes but also two rotary axes A and B (or A and C, or B and C), which allow the workpiece or cutting tool to be rotated along X and Y (or X and Z, or Y and Z) axes respectively. Fig. 1-1 shows a 5-axis Deckel Maho DMU 60T CNC machine center with X, Y, Z linear axes and B, C rotation axes.

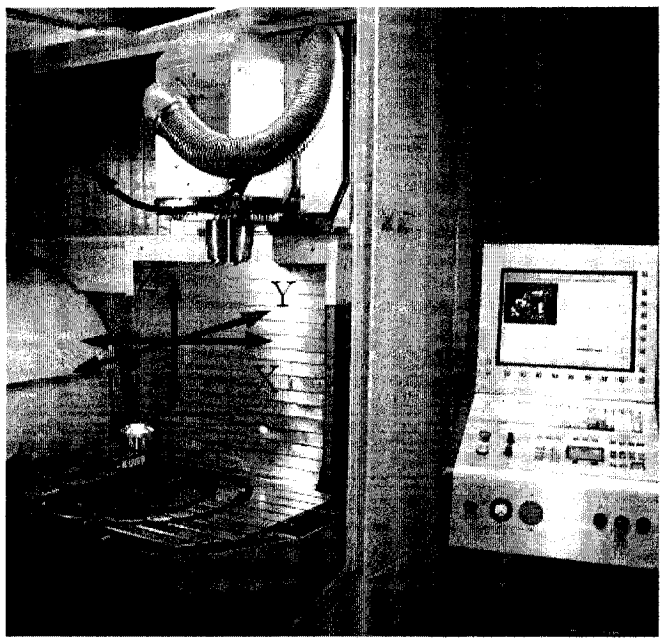

Figure 1-1: Five-axis Deckel Maho DMU 60T CNC machining center

1.2 CNC milling for free-form surfaces

1.2.1 Free-form surface

Free-form surface (sculptured surface) was initially developed for the automotive and aerospace industries, and now free-form surfacing is widely used in all engineering design disciplines from consumer goods products to ships. Mathematically, sculptured surfaces are represented with a type of non-periodic uniform rational B-spline (NURBS) surface, which is an industrial standard in CAD and other computer graphics software to describe complex geometric shapes, such as turbine blades, car bodies and boat hulls.

The advantages of using NURBS include:

- Any curve or surface can be formulated using NURBS. The NURBS model is considered as a unified canonical representation that can define both synthetic (Bezier, B-splines) and analytic (circles and conics) curves and surfaces.
- Their related algorithms are stable and accurate.
- They reduce computer memory consumption in describing geometric shapes.
- They are easy to use in design and geometric modeling.

The complicated part shapes can be designed using the NURBS surfaces in CAD software, which are stored with their control points, orders of base functions, knot vectors and weights. Fig. 1-2 shows a free-form surface and its control points. Number of control points is independent with the orders of the NURBS surface.

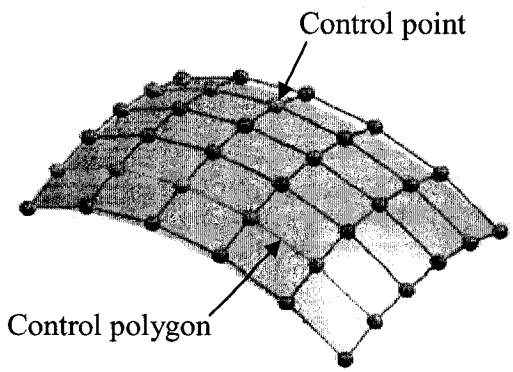

Figure 1-2: Free-form surface and its control points

Commonly, many surface patches are needed to form a part shape. The smoothness between patches is often defined in terms of continuity.

- positional continuity (C^0): the end positions of two curves or surfaces are coincidental. The curves or surfaces may meet with angle, giving rise to a sharp corner or edge.
- tangential continuity (C^1): the end vectors of two curves or surfaces are parallel.
- curvature continuity (C^2): the surface patches are curvature continuous to each other.

Sometimes, to ensure aerodynamic requirements for a sculptured part, it has to be designed by using NURBS patches with at least C^2 continuity.

1.2.2 End-mills

End-mills are cutters commonly used for free-form surface milling. Three typical end-mills are flat, ball and bull-nose end-mills as shown in Fig. 1-3. Flat end-mills are often used in roughing because of its high material remove rate. Bull-nose end-mills offer some advantages over ball end-mills. During machining, the cutting speed at the tip of a ball end-mill is zero, resulting dull appearance on part surfaces.

End-mills have traditionally been made from high speed steel, and now some are made from tungsten carbide, a rigid and wear-resistant material. These tungsten carbide end-mills are manufactured through pressing carbide powder into rods and grinding into blanks of industry-standard sizes. It is becoming popular in industry to replace traditional solid end-mills by more cost-effective cutting tools with inserts, which, though more expensive initially, can reduce tool-change time and allow easy replacement of worn or broken cutting edges, rather than the entire cutter. Coatings are also widely used to reduce wear and friction.

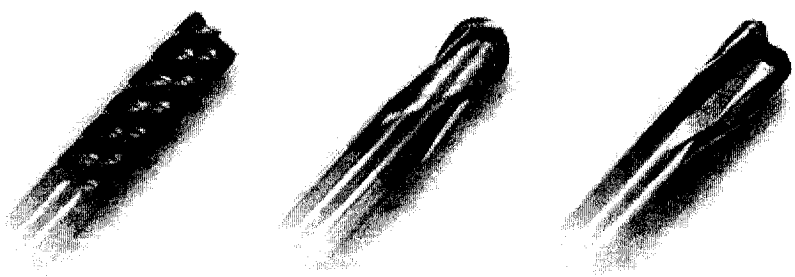

(a) (b) (c)

Figure 1-3: (a) Flat end-mill, (b) ball end-mill, and (c) bull end-mill

1.2.3 Part set-up in 3- and 4-axis milling

For 3-axis sculptured surface machining, the cutter can move simultaneously along X, Y and Z axes. Fig. 1-4 shows a hair dryer mold is set up on a 3-axis vertical milling machine.

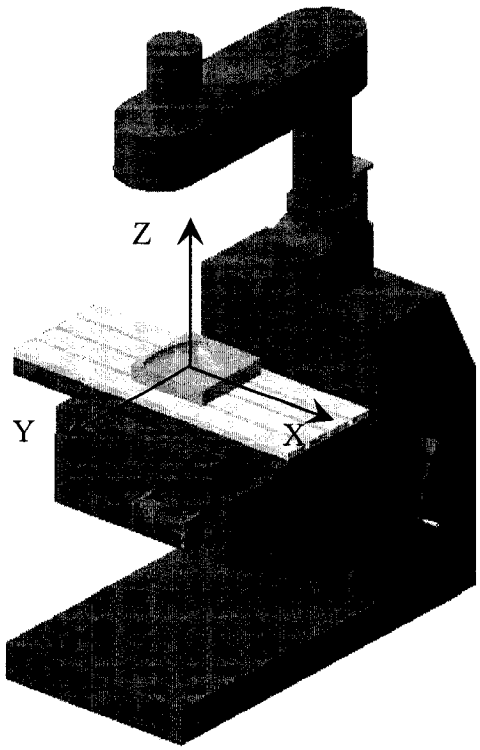

Figure 1-4: Example of a hair dryer mold, which is set up in 3-axis CNC machining

Several types of parts can only be machined on 4-axis mill. For example, certain types of axial-flow rotors, their blades and hub are integrated into one single piece, which is cut from a disk-like stock on 4-axis CNC machines. Because of the complex geometries of the pressure and suction sides and the small pitch space among the blades, the blades cannot be machined by using 3-axis CNC machines. Usually, the workpiece is machined with 4-axis CNC milling, in which it is fixed on a rotary table with their central axes coinciding with each other (see Fig. 1-5). The axis of the rotary table fixed on the machine table is aligned with either x- or y-axis of the machine tool. In this work, it is assumed that a 4-axis horizontal milling machine is

used, in which the cutter moves along z-axis, and the axis of the rotary table is aligned with y-axis of the machine coordinate system. Thus, the workpiece can be rotated along the y-axis by angle B; by changing the angle B, the relative orientation between the cutter and the part is changed so that all CC points can be accessed, and the angle B represents the cutter orientation.

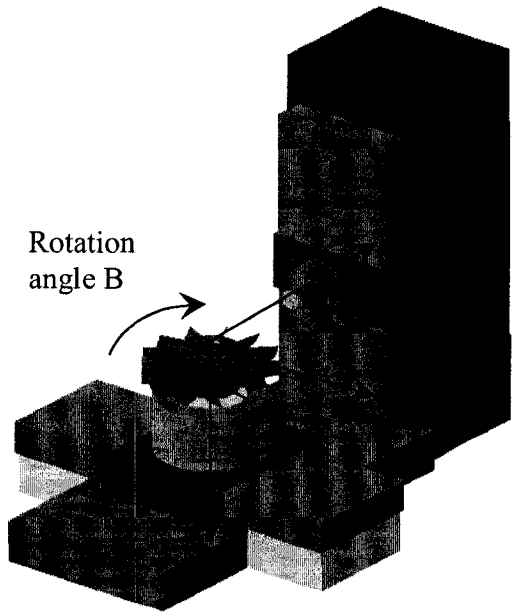

Figure 1-5: Example of an axial-flow compressor, which is set up in 4-axis CNC machining

Based on the above set-up configurations, a workpiece coordinate system is established on the part, shown in Fig. 1-4 and Fig. 1-5, and the part design has to be transferred from the design coordinate system, if different, into the workpiece coordinate system, where CNC tool-paths will be planned.

1.2.4 Machining processes

Sculptured surface milling usually includes four stages, each of which is implemented by a variety of basic and sophisticated strategies, depending on the material, the part shape and required machining tolerance. These stages are:

- Roughing

This process begins with raw stock, and cuts it very roughly to shape of the final model. This is the first stage of machining where the object is to quickly remove the bulk of the waste material.

- Semi-finish

This process begins with a roughed part that unevenly approximates the model and cuts to within a fixed offset distance from the model. The semi-finishing pass must leave a small amount of material so the cutter can cut accurately while finishing.

- Finish

This stage involves a slow pass across the material in very fine steps to produce the finished part. In finishing, the step between one pass and another is minimal. Feed rates are low and spindle speeds are raised to produce an accurate surface. So, it is the longest process of all.

- Clean-up

This stage is to clean-up the un-cuts with smaller cutters. Fillet-cut and pencil-cut belong to this stage.

No matter which machining process is used, the free-form surface milling is a "point" milling process where a sequence of cutter-contact (CC) points is traced by end-mills. The pattern of "tracing" is called the tool-path topology. There are four types of tool-path topology patterns: (1) serial-pattern, (2) radial-pattern, (3) strip-pattern, and (4) contour-pattern. Once tool-path topology patterns are determined, a CC point mesh on the sculptured surface can be created in the following ways: the sequent CC points on the same tool-path are generated with chordal derivation less than the specified machining tolerance; the distance between two adjacent tool-paths should let the scallop height less than a specified value.

Then, cutter type and size are selected and cutter orientation is determined for each CC point to prevent machined part from gouging and interference, and at the same time, to achieve a high surface quality. In the sculptured surface machining, big cutters has some advantages: (1) reduce the number of CC points through adopting a larger distance between two adjacent tool paths, hence reach a high machining efficiency, and (2) increase the cutter rigidity and reduce the tool vibration. To using a big tool in the sculptured surface machining, the first thing needed to consider is gouging and interference avoidance.

1.2.5 Gouging and interference

Gouging and interference-free machining is a critical requirement in the sculptured surface machining, because gouging and interference can damage the machine tool

and workpiece. Gouging occurs on a part's surface when the cutting tool cuts into the design surface near a CC point (see Fig. 1-6). This defect is caused by an in-appropriate cutter size. If the curvature of the cutting surface of the end-mill is less than that of the part surface being machined at a CC point, the part surface will be gouged locally. Interference between a tool and a workpiece refers to that the tool shank collides with the workpiece during cutting (see Fig. 1-7). This results from an improper cutter orientation.

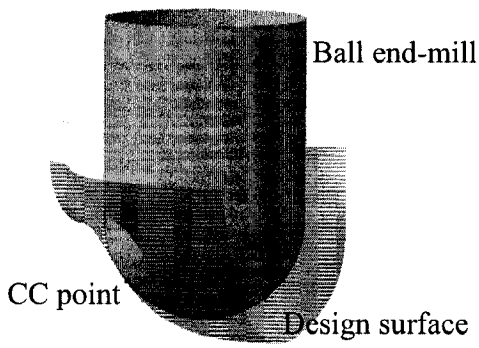

Figure 1-6: Gouging: a ball end-mill cuts into the design surface

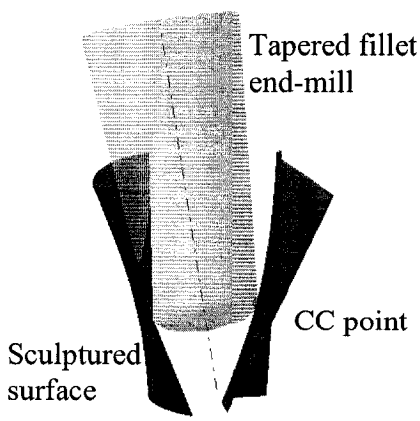

Figure 1-7: Interference: the shank of a bull-nose end-mill interferes with one design surface

Gouging and Interference problems are the main obstacle to ensuring machining precision and efficiency in the multi-axis CNC machining of free-form surfaces. Commonly, a small cutter is selected and machining efficiency is sacrificed to meet the machining accuracy requirements. Using conventional methods to determine cutter size and orientation, gouging and interference detections are separated. First, cutter size is determined to avoid the local gouging in terms of the curvature comparison or the distance calculation between the cutting surface and the designed surface at same CC point. Then, the interference is checked based on this no-gouging cutter size. If the interference occurs, the cutter size or orientation is adjusted accordingly. The check and the orientation adjustment may repeat several times until a satisfied cutter size and orientation are chosen. So, these methods are time-consuming, also, the determined cutter size and orientation may not be optimal, then, the high machining efficiency will lose.

1.3 Literature review

Among the publicized tool-selection research [1-5], Jesen *et al.* [1] proposed an automatic cutter size selection methodology for five-axis surface finish machining based on the curvature matching technique. This method optimizes cutter orientations, provides close-form equations to determine the shank and corner radii of cutting tools, and presents simple algorithms to detect and prevent local and global tool gouging. Glaeser *et al.*, [2] mathematically described the concept of exhaustive curvature comparison and presented local and global conditions for 3-axis collision-free milling of sculptured surfaces. Lo [3] planned tool paths for ball end-milling of concave and wall-bounded

surfaces in two stages: (1) a larger cutter is used to efficiently machine the majority part of the surface; and (2) a smaller cutter machines the rest, whose size is minimized. Lee and Chang [4] applied the maximum effective cutting radius approach to cutter selection for 5-axis surface machining. Yang and Han [5] located iso-phote curves on the sculptured surfaces to find the patches accessible in 3-axis machining and selected a number of cutting tools for the minimum machining time. However, none of these approaches can effectively determine the maximum allowable cutter size for 3-axis finish machining of compound surfaces.

Since the cutter size determination is actually to detect gouging, the related articles [6-11] and [19-27] have been reviewed. Yoon *et al.* [6] proposed a local condition for 5-axis collision-free milling based on the Taylor's quadratic approximations of the cutter and part surfaces in the vicinity of a cutter-contact point. Later he [7] introduced the concept of machined region width to optimize the cutter orientation for 5-axis machining. Since he assumed that these approximations were accurate in a large area, which is not true, these works are impractical. Rao and Sarma [8] applied the curvature comparison technique to the part and cutter-swept surfaces in order to detect local gouging when using flat end-mills in 5-axis machining. Wang and Yu [9] determined the cutter orientation along the minimum curvature direction for wider machining strips and carried out rough inspection for gouging. Unfortunately, detailed inspection for bull-nose end-mills was not conducted in these two research works. George and Babu [10] found the self-intersection curves of the cutter location surface by applying optimization techniques and solving differential equations and deleted the locations that cause local gouging.

Hatna and Grieve [11] pre-processed the surface in order to discard the zones of potential interference and generated interference-free tool paths in a simple sweeping process of the surface parametric space. These methods either cannot accurately detect local gouging or are very tedious in computation.

1.4 Thesis objectives

To conduct multi-axis sculptured surface machining, cutter sizes and orientations are directly related to surface quality and cutting efficiency; more specifically, using cutters with optimal sizes and orientations can effectively avoid gouging and interference and efficiently remove stock material during machining. In practice, if a larger cutter is selected, it may over-cut the sculptured surface in some regions, even though it can form the surface shape quickly. On the other hand, if a smaller cutter is adopted, it can remove the stock material without cut into the design surface; however, it will take a longer time to produce the surface part and the manufacturing cost will increase. In multi-axis CNC machining, the cutter can collide the workpiece at its shank if it accesses the part along an improper direction. It is very difficult to determine the optimal cutter orientation manually. Unfortunately, the existing CAD/CAM software systems cannot provide effective solutions to determine optimal cutter sizes and cutter orientations for multi-axis sculptured surface machining.

To address the present problems, the first objective of this work is to propose a generic, effective method for determining the optimal cutter sizes and cutter orientations

for 3- and 4-axis milling of free-form surfaces. The literature review has revealed that the existing methods for cutter size and orientation determination can be divided into two groups: (1) local gouging avoidance through curvature comparison; and (2) gouging and interference avoidance by checking the minimum distance between the tool's cutting surface and the part's design surface. First, these methods subjectively select cutter sizes and orientations and, second, visually inspect for gouging and interference using machining simulation. If gouging and interference are detected, either the cutter sizes or the cutter orientations have to be changed. Then repeat the gouging and interference detection and the cutter size and orientation adjustment, until proper cutter sizes and orientations are found. As a result, these methods are time-consuming. Hence, a new methodology that can effectively determine cutter sizes and orientations is needed in industry. My thesis research is to propose a new method for formulating optimal cutter sizes and orientations with a global optimization model.

To quickly find solutions of the above-mentioned model, the second objective of my research work is to develop an efficient global optimization solver. Among many established solvers, the genetic algorithm (GA), particle swarm optimization (PSO) and simulating annealing (SA) methods are quite popular, even though they are less efficient or not stable. The well-established local optimization methods can pinpoint the optimum quickly, if the objective function is either convex or concave. If a hybrid optimization method works in such a way, global search for the local region where the optimum locates using the global method and fast convergence to the optimum using the local method, a global optimization problem can be efficiently solved. To take this advantage,

my research will develop a hybrid global optimization method in order to solve the complicated model of optimal cutters and orientations.

1.5 Thesis outline

This thesis comprises six chapters. Chapter one introduces some basic concepts about the CNC machining, free-form surface machining, research problems, literature review and thesis objectives. Chapter two presents a new method to formulate close-form equations of an imaginary cutter size at one cutter-contact point and then establishes an optimization model to represent the allowable cutter size (the minimum among all imaginary cutter sizes at the CC point). Chapter three describes a new optimization method, the hybrid global optimization method, to synthesize the particle swarm optimization method (PSO) and the gradient optimization method and compares this method to other popular methods. In Chapter four and five, this new approach is applied to two industrial examples, one is the 3-axis milling of a hair dryer mold with 24 sculptured surface patches; another one is 4-axis milling of the airfoils of an axial-flow compressor. In these examples, a group of standard, optimal cutters and their orientations are used in machining to achieve a high efficiency. Chapter six highlights the significance and contributions of this research work and future work of this research.

Chapter 2 Mathematical Model of the Allowable Cutter Size for a CC Point

2.1 Compound surface

In CAD software systems, sculptured surfaces of mechanical parts are uniquely modeled with non-uniform rational B-spline (NURBS) surfaces, which are usually represented in parametric form as

$$\mathbf{P}(u,v) := \frac{\sum_{k=0}^{\#u}\sum_{l=0}^{\#v} w_{k,l}\cdot \mathbf{C}_{k,l}\cdot N_{k,\deg\_u}(u)\cdot N_{l,\deg\_v}(v)}{\sum_{k=0}^{\#u}\sum_{l=0}^{\#v} w_{k,l}\cdot N_{k,\deg\_u}(u)\cdot N_{l,\deg\_v}(v)},\quad (u,v)\in[u_{\min},u_{\max};v_{\min},v_{\max}], \tag{2.1}$$

where u and v are the surface parameters, and their domain is denoted as $\Re^2 := [u_{\min},u_{\max};v_{\min},v_{\max}]$. $\mathbf{C}_{k,l}$ $(k = 0,\ 1,\ ...,\ \#u;\ l = 0,\ 1,\ ...,\ \#v)$ are the control points, and $w_{k,l}$ are their corresponding weights. $N_{k,\deg\_u}(u)$ and $N_{l,\deg\_v}(v)$ are the base functions. These data of each NURBS surface and its boundaries are stored in the CAD systems.

To design a part of complex shape, a compound surface is often used. It is a group of NURBS surface patches connected with either position (C^0), tangent (C^1), or curvature

(C^2) continuity between them. These surface patches are represented as $\mathbf{S}_i$ $(i = 0, 1, ..., m)$, and a point on them is expressed as $\mathbf{P}(u,v) \in \mathbf{S}_i$, $(i = 0, 1, ..., m)$. If the domain of patch $\mathbf{S}_i$ is denoted as $\Re_i^2 := [u_{i,\min}, u_{i,\max}; v_{i,\min}, v_{i,\min}]$, the domain of the compound surface can be $\Re^2 = \Re_1^2 \cup \Re_2^2 \cup ... \Re_i^2 \cup ... \Re_m^2$. Thus, we have $(u,v) \in \Re^2$. These surface patches form a compound surface, thus the part is called a compound surface part, which can be denoted as $\mathbf{S} := \mathbf{S}_1 \cup \mathbf{S}_2 \cup ... \mathbf{S}_i \cup ... \mathbf{S}_m$. In CAD systems, the data of all the surface patches on a compound surface are stored, and they are connected in the database with the borders between the surfaces. Thus, with regard to any surface patch, it is easy to identify its neighbouring surface patches automatically in determining the maximum cutter size for CNC machining.

2.2 Representation of APT cutter geometry

In the CNC milling of sculptured surfaces, standard flat, ball, or bull-nose end-mills are often used, which are three special cases of the generic ISO APT cutter. The APT cutter and the end-mills with their geometric parameters are illustrated in Fig. 2-1. Usually, the imaginary envelope formed by the blades in cutter spinning is called cutting surface. For the APT cutter, the cutting surface thus consists of a tapered (A-B), a fillet (B-C), and a conical (C-O) surface. In practice, the taper angle θ is between zero to 20 degrees, and the conical angle ψ is small. Parameter r is the radius of the corner, R is the radial distance between the cutter axis and the center of the corner, and H is the cutter length.

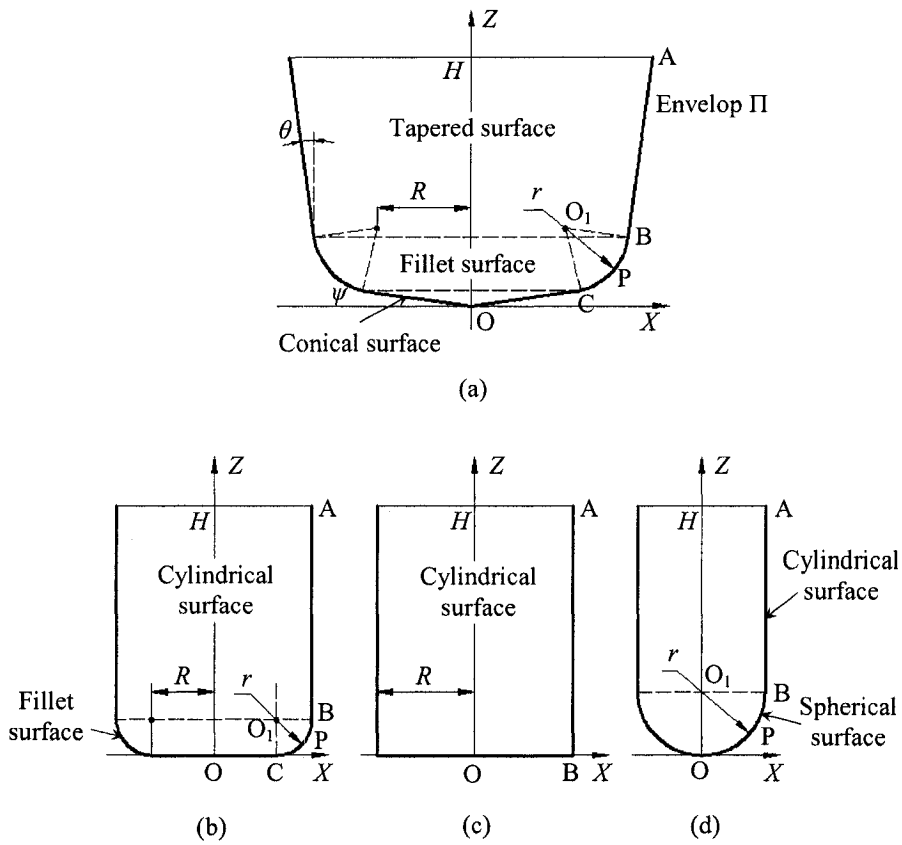

Figure 2-1: (a) An APT cutter, (b) a bull-nose end-mill, (c) a flat end-mill, and (d) a ball end-mill

To represent the cutting surface of the APT cutter, a tool coordinate system is established with its origin at the cutter tip and its Z-axis as the tool axis (see Figure 1(a)). The coordinates of point C are $[x_C, z_C] = [R + r \cdot \sin\psi, (R + r \cdot \sin\psi) \cdot \tan\psi]$, and The conical surface can be represented in a parametrical form as

$$\mathbf{T}(z,\alpha) = \begin{bmatrix} \dfrac{\cos\alpha}{\tan\psi} \cdot z \\ \dfrac{\sin\alpha}{\tan\psi} \cdot z \\ z \end{bmatrix}, \quad z \in [0,\ z_C] \tag{2.2}$$

The coordinates of point O_1 are $[x_{O_1},\ z_{O_1}] = [R,\ R \cdot \tan\psi + r \cdot \sec\psi]$, and those of point B are $[x_B,\ z_B] = [R + r \cdot \cos\theta,\ R \cdot \tan\psi + r \cdot \sec\psi - r \cdot \sin\theta]$. Thus, the fillet surface can be represented in a parametric form as

$$\mathbf{T}(z,\ \alpha) = \begin{bmatrix} \left[R + \sqrt{r^2 - (z_{O_1} - z)^2}\right] \cdot \cos\alpha \\ \left[R + \sqrt{r^2 - (z_{O_1} - z)^2}\right] \cdot \sin\alpha \\ z \end{bmatrix}, \ z \in [z_C,\ z_B] \tag{2.3}$$

The coordinates of point A are $[x_A,\ z_A] = [R + r \cdot \cos\theta + H \cdot \tan\theta,\ H]$. The tapered surface can be represented in a parametric form as

$$\mathbf{T}(z,\ \alpha)=\begin{bmatrix}\left[x_B+(z-z_B)\cdot\tan\theta\right]\cdot\cos\alpha\\ \left[x_B+(z-z_B)\cdot\tan\theta\right]\cdot\sin\alpha\\ z\end{bmatrix},\ z\in[z_B,\ z_A] \tag{2.4}$$

where parameter α is an angle measured from X-axis on XOY plane of the tool coordinate system, and its range is $[0,\ 2\pi]$.

An APT cutter becomes a bull-nose end-mill when $\theta=0$ and $\psi=0$ (see Fig. 2-1(b)); a flat end-mill when $\theta=0$, $\psi=0$ and $r=0$ (see Fig. 2-1(c)); and a ball end-mill when $\theta=0$, $\psi=0$ and $R=0$ (see Fig. 2-1(d)).

To efficiently machine sculptured surfaces, a group of the standard end-mills in different sizes are often used to access different regions. In industry, the taper angle φ of these cutters is fixed at one of several small degrees (such as 1°, 3°, 5°, 7° and 10°), and cutters with conical angle $\psi=0$ are often used in practice. Furthermore, since the corner radius r of the bull-nose end-mills is usually fixed at $\frac{1}{32}$, $\frac{1}{16}$, or $\frac{1}{8}$ inches by tool manufacturers, in this work, the corner radius r of the bull-nose end-mills are initially determined with those values. Therefore, R of the bull-nose and flat end-mills and r of the ball end-mills are subject to change and should be determined.

2.3 Mathematical model of the allowable cutter size at a CC point

2.3.1 Theorem for allowable cutter size

A salient geometric feature of compound surfaces is that the surfaces are complex in shape and the open space for the cutter to access a part surface to be machined, $\mathbf{S}_0$, is reduced by this part surface and the neighbouring surfaces, called checking surfaces $\mathbf{S}_i \ (i = 1, 2, ..., n)$. Consequently, gouging and interference between the cutter and the part often occur in machining, which should be the major problem to be addressed in NC tool-path planning for the compound surface machining. To solve this problem, a theorem is provided.

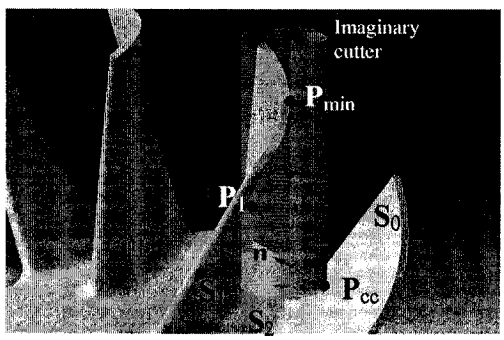

Figure 2-2: Illustration of the model of allowable cutters

In Fig. 2-2, suppose in the geometry of a part, a point $\mathbf{P}_{CC}$ on a bounded surface $\mathbf{S}_0$ to be cut is accessible in a part set-up, even if there are some bounded, check surfaces $\mathbf{S}_i \ (i = 1, 2, ..., n)$, which are adjacent and facing this surface. An imaginary cutter – APT cutter in variable size R or r – can be constructed, if possible, under two principles: (1) the fillet cutting surface of the cutter envelop $\Pi(r)$ is

tangent to surface $\mathbf{S}_0$ at point $\mathbf{P}_{CC}$, and (2) this envelop passes through any other point $\mathbf{P}$ (called testing point) on these surfaces $\mathbf{S}_i$ $(i = 0, 1, 2, ..., n)$, therefore, the smallest (called the allowable cutter) among all imaginary cutters can machine surface $\mathbf{S}_0$ at point $\mathbf{P}_{CC}$ without gouging and interference.

Proof: According to the two principles, a feasible imaginary cutter cannot be determined at some points, $\mathbf{P}$; however, if positive, the cutter is uniquely defined. In the following proof, only feasible cutters are considered.

(1) Only $\mathbf{S}_0$ is considered. If some testing points, $\mathbf{P}_1$, on $\mathbf{S}_0$ can determine an APT cutter, its envelope Π_1 would intersect this surface in an interior area $\mathbf{O}_1$ of $\mathbf{S}_0$, which is represented as

$$\Pi_1 \cap \mathbf{S}_0 = \{\mathbf{P}_{CC}, \mathbf{P}_1, \mathbf{O}_{1,j}\}$$

By changing the location from $\mathbf{P}_1$ to $\mathbf{P}_2$, the new envelope can intersect this surface in a smaller area $\mathbf{O}_2$, and the cutter size R or r is reduced. Theoretically, by searching all points $\mathbf{P}_k$ on $\mathbf{S}_0$, a smaller cutter can be found one step after another, and the intersection area is reduced accordingly.

$$\Pi_k \cap \mathbf{S}_0 = \{\mathbf{P}_{CC}, \mathbf{P}_k, \mathbf{O}_k\};\ \mathbf{O}_k < \mathbf{O}_{k-1} \text{ and } R_k < R_{k-1} \text{ or } r_k < r_{k-1}$$

It is always true that when the interior intersection area converges to a point, the cutter size R or r reaches the minimum $R_{\min}(\mathbf{S}_0, \mathbf{S}_0)$ or $r_{\min}(\mathbf{S}_0, \mathbf{S}_0)$ and this point is denoted as $\mathbf{P}_{\min}$. Physically, the cutter is tangent to $\mathbf{S}_0$, if $\mathbf{P}_{\min}$ is an interior point; or touches a boundary of $\mathbf{S}_0$, if $\mathbf{P}_{\min}$ is on it. Therefore, it would not gouge or interfere with $\mathbf{S}_0$. Specifically, if $\mathbf{P}_{\min} \rightarrow \mathbf{P}_{CC}$, $\Pi_{\min}(\mathbf{S}_0) \cap \mathbf{S}_0 = \mathbf{P}_{CC}$, it indicates that the gouge-free cutter is smaller than the interference-free cutter; otherwise, if $\mathbf{P}_{\min}$ is away from $\mathbf{P}_{CC}$, the interference-free cutter is smaller than the gouge-free cutter.

(2) $\mathbf{S}_0$ and $\mathbf{S}_1$ are considered. If the testing point $\mathbf{P}$ is taken from these two surfaces and the optimal point is on $\mathbf{S}_1$, the corresponding cutter size is minimum $R_{\min}(\mathbf{S}_0, \mathbf{S}_1)$ or $r_{\min}(\mathbf{S}_0, \mathbf{S}_1)$, which would not gouge or interfere with these two surfaces.

(3) $\mathbf{S}_0$ and $\mathbf{S}_2$ are considered. Similar to Step 2, the optimal point can be found and the minimum cutter size is $R_{\min}(\mathbf{S}_0, \mathbf{S}_2)$ or $r_{\min}(\mathbf{S}_0, \mathbf{S}_2)$. Thus, the minimum cutter sizes for all the other pairs of surfaces can be calculated as $r_{\min}(\mathbf{S}_0, \mathbf{S}_3)$, ..., $r_{\min}(\mathbf{S}_0, \mathbf{S}_n)$.

(4) It is easy to understand that the minimum $R_{\min}$ or $r_{\min}$ of all the minimum cutters calculated, $R_{\min}(\mathbf{S}_0, \mathbf{S}_0)$ or $r_{\min}(\mathbf{S}_0, \mathbf{S}_0)$, $R_{\min}(\mathbf{S}_0, \mathbf{S}_1)$ or $r_{\min}(\mathbf{S}_0, \mathbf{S}_1)$, ..., $R_{\min}(\mathbf{S}_0, \mathbf{S}_n)$ or $r_{\min}(\mathbf{S}_0, \mathbf{S}_n)$, will not gouge and interfere with any of these surfaces.

So this cutter is called the allowable cutter to machine $\mathbf{S}_0$ at the CC point without gouging and interference.

To establish the cutter model for the allowable cutter size based on the above-mentioned two principles, first, assume a part to be machined on a 3-axis CNC milling machine. In this part, a CC point $\mathbf{P}_{CC} = [x_{CC}, y_{CC}, z_{CC}]^T$ is on the surface $\mathbf{S}_0$ to be cut, and the testing point $\mathbf{P} = [x, y, z]^T$ is either on this surface or check surfaces $\mathbf{S}_i$ $(i = 1, 2, ..., n)$. The unit surface normal $\mathbf{n} = [n_x, n_y, n_z]^T$ can be easily calculated, and the corner radius r, taper angle φ and conical angle ψ are specified. An imaginary APT cutter can be uniquely determined so that its envelope touches surface $\mathbf{S}_0$ at the CC point and passes the testing point. The radial parameter R or r representing the cutter size can be determined with the following models.

2.3.2 Imaginary cutter size model for the general APT cutters

Suppose APT cutters are to be used in machining, we can initially assign to parameters θ, ψ, and r of these cutters with the specification values of the standard cutters available in the market, so R is the only parameter has to be determined as the imaginary APT cutter size. Set $\Delta x := x - x_{CC} - \mathrm{r} \cdot n_x$, $\Delta y := y - y_{CC} - \mathrm{r} \cdot n_y$, $\Delta z := z - z_{CC} - \mathrm{r} \cdot n_z$, $\lambda := 1/\sqrt{n_x^2 + n_y^2}$. According to the following conditions for z

value of the testing point **P**, parameter R can be computed and then cutter diameter can be calculated accordingly.

$$D = 2 \cdot R + \frac{2 \cdot \mathrm{r} \cdot \sin\left(\frac{\pi}{4} - \frac{\theta}{2} + \frac{\psi}{2}\right)}{\cos\left(\frac{\pi}{4} - \frac{\theta}{2} - \frac{\psi}{2}\right)} \tag{2.5}$$

Fig. 2-3 shows a general APT cutter and its two extreme cases when radius R is zero or infinite large. For a feasible imaginary APT cutter (R is positive), its cutting envelop comprises three portions: a tapered surface (**TS**), a fillet surface (**FS**) and a conical surface (**CS**). These portions will shrink to $\mathbf{TS}_0$, $\mathbf{FS}_0$ and $\mathbf{CS}_0$ or extend to $\mathbf{TS}_\infty$, $\mathbf{FS}_\infty$ and $\mathbf{CS}_\infty$ respectively when R equals zero or infinite large. The cutting envelop of every feasible imaginary cutter is inside the volume bounded by $\mathbf{TS}_0$, $\mathbf{FS}_0$ & $\mathbf{CS}_0$ and $\mathbf{TS}_\infty$, $\mathbf{FS}_\infty$ and $\mathbf{CS}_\infty$. Then, if a testing point **P** is outside this volume, there is no feasible imaginary cutter existing, however, if a testing point **P** is inside this volume, a feasible imaginary cutter can always be found. To judge which portion of the cutting envelop will touches the testing point **P**, two planes $\mathbf{PL}_1$ and $\mathbf{PL}_2$ are used and shown in Fig. 2-4. $\mathbf{PL}_1$ is the plane on which the intersection circle between **TS** and **FS** locates. $\mathbf{PL}_2$ is a plane on which the intersection circle between **FS** and **CS** locates. Because only R is the variable in this model, $\mathbf{PL}_1$ and $\mathbf{PL}_2$ will keep invariant from changing R. If **P** is above $\mathbf{PL}_1$, only the tapered surface has chance to touch **P**. If **P** is between $\mathbf{PL}_1$ and $\mathbf{PL}_2$, **P** can only locate on the fillet surface. If **P** is below $\mathbf{PL}_3$, only the conical surface will pass **P**. Then, the imaginary cutter size can be calculated through the following equations.

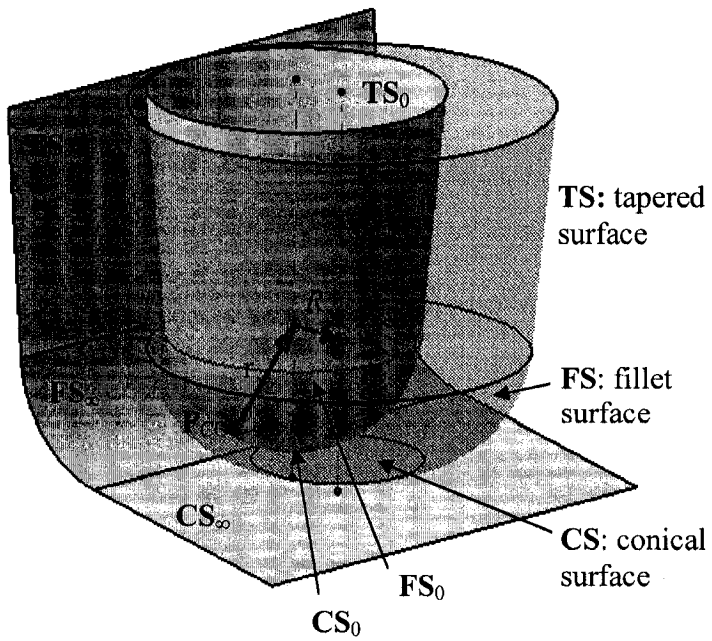

Figure 2-3: Example of imaginary cutter and its two extreme case: R=0 or R=∞.

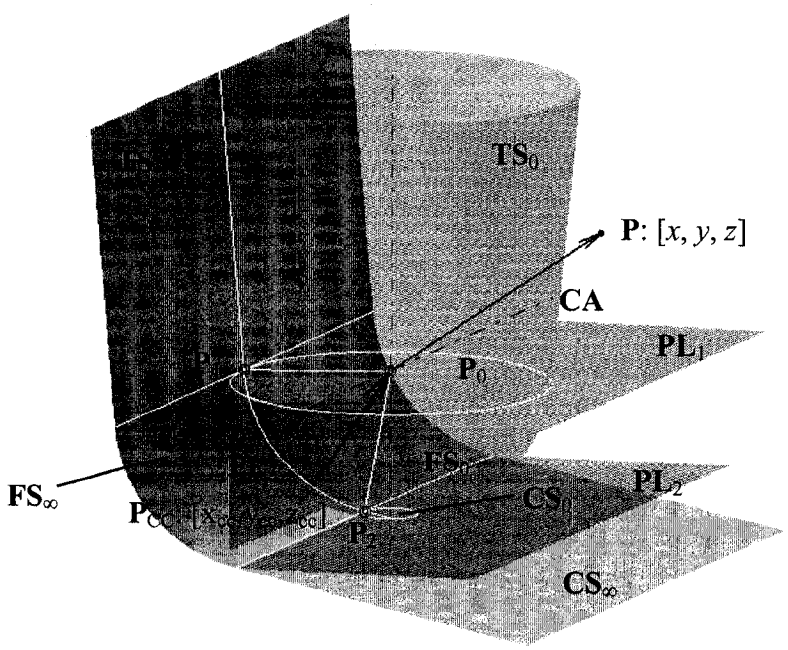

Figure 2-4: Some geometry features used in imaginary cutter model.

Condition 1: $\Delta z \geq -r \cdot \sin\theta$

In this condition, the testing point **P** is above the plane $\mathbf{PL}_1$. So, only the tapered surface **TS** can touch **P**. There are three cases existing in terms of the location of the testing point.

- Case 1

If **P** is inside the volume bounded by $\mathbf{TS}_0$, no matter what R is, **P** will be gouged. Then, R can be set as 0. All satisfied testing points can be expressed as:

$$\Delta x^2 + \Delta y^2 \leq \left(\Delta z \cdot \tan\theta + r \cdot \sec\theta\right)^2 \tag{2.6}$$

- Case 2

If **P** locates on the opposite side of the plane $\mathbf{TS}_\infty$ where the cutter locates, no matter what R is, **P** will not be gouged. Then, R can be set as ∞. The criterion that determine these testing points is derived as follows:

Surface normal of $\mathbf{TS}_\infty$ is $\mathbf{P}_0\mathbf{P}_1$, so, **P** should satisfy the inequality equation:

$$\overrightarrow{\mathbf{P}_1\mathbf{P}} \times \overrightarrow{\mathbf{P}_1\mathbf{P}_0} \leq 0 \tag{2.7}$$

$$\left(\begin{bmatrix} x \\ y \\ z \end{bmatrix} - \begin{bmatrix} x_{cc} + r \cdot n_x + r \cdot \lambda \cdot n_x \cdot \cos\theta \\ y_{cc} + r \cdot n_y + r \cdot \lambda \cdot n_y \cdot \cos\theta \\ z_{cc} + r \cdot n_z - r \cdot \sin\theta \end{bmatrix}\right) \cdot \begin{bmatrix} \lambda \cdot n_x \cdot \cos\theta \\ \lambda \cdot n_y \cdot \cos\theta \\ \sin\theta \end{bmatrix} \leq 0 \tag{2.8}$$

Ineq. (2.8) can be simplified as:

$$\lambda \cdot n_x \cdot \Delta x \cdot \cos\theta + \lambda \cdot n_y \cdot \Delta y \cdot \cos\theta + \Delta z \cdot \sin\theta + r \le 0 \tag{2.9}$$

- Case 3

If **P** is in the volume bounded by $\mathbf{TS}_0$ and $\mathbf{TS}_\infty$, there always exists an feasible imaginary cutter whose cutting surface contacts the $\mathbf{P}_{CC}$ and at the same time touches **P**, the following equation can be obtained:

$$\begin{aligned}&\left[x-\left(x_{CC}+r\cdot n_x+R\cdot\lambda\cdot n_x\right)\right]^2+\left[y-\left(y_{CC}+r\cdot n_y+R\cdot\lambda\cdot n_y\right)\right]^2=\\&\left\{R+r\cdot\cos\theta+\left[z-\left(z_{CC}+n_z\cdot r-r\cdot\sin\theta\right)\right]\cdot\tan\theta\right\}^2\end{aligned} \tag{2.10}$$

From Eq. (2.10), parameter R can be calculated:

$$R=\frac{1}{2}\cdot\frac{\Delta x^2+\Delta y^2-\left(\Delta z\cdot\tan\theta+r\cdot\sec\theta\right)^2}{\lambda\cdot n_x\cdot\Delta x+\lambda\cdot n_y\cdot\Delta y+\Delta z\cdot\tan\theta+r\cdot\sec\theta} \tag{2.11}$$

Condition 2: $-r\cdot\cos\psi < \Delta z < -r\cdot\sin\theta$

In this condition, **P** is between the planes $\mathbf{PL}_1$ and $\mathbf{PL}_2$. Only the fillet surface can touch **P**. There are also three cases existing in terms of the location of the testing point **P**.

- Case 1

If **P** is in the volume bounded by $\mathbf{FS}_0$, **P** will be gouged. Then, R can be set as 0. All satisfied points can be expressed as:

$$\Delta x^2 + \Delta y^2 + \Delta z^2 \le r^2 \tag{2.12}$$

- Case 2

If **P** locates on the opposite side of $\mathbf{FS}_\infty$ where the cutter locates, **P** will not be gouged. Then, R can be set as ∞. The criteria can be derived as follows:

Criterion one: **P** should be outside the cylinder surface $\mathbf{FS}_\infty$.

In Fig. 2-4, $\mathbf{FS}_\infty$ is a cylinder surface, and we use **CA** to represent its axis. $\mathbf{PL}_3$ is a reference plane which is passing through **CA** and perpendicular with the horizontal plane XY. If there exists a point $\mathbf{P}_p$ on the cylinder axis **CA** and $\overrightarrow{\mathbf{P}_p\mathbf{P}}$ is perpendicular with **CA**. Then, if $\left|\overrightarrow{\mathbf{P}_p\mathbf{P}}\right| \ge r$, **P** will not be gouged.

CA can be written as:

$$\begin{bmatrix} x_{cc} + n_x \cdot r - n_y \cdot t \\ y_{cc} + n_y \cdot r + n_x \cdot t \\ z_{cc} + n_z \cdot r \end{bmatrix} \tag{2.13}$$

Here, t is a variable.

Because $\overrightarrow{\mathbf{P}_p\mathbf{P}} \perp \mathbf{CA}$, we have

$$\left(\begin{bmatrix} x \\ y \\ z \end{bmatrix} - \begin{bmatrix} x_{CC} + n_x \cdot r - n_y \cdot t \\ y_{CC} + n_y \cdot r + n_x \cdot t \\ z_{CC} + n_z \cdot r \end{bmatrix} \right) \cdot \begin{bmatrix} -n_y \\ n_x \\ 0 \end{bmatrix} = 0 \tag{2.14}$$

From Eq. (2.14), t can be obtained,

$$t = \frac{n_x \cdot \Delta y - b \cdot \Delta x}{n_x^2 + n_y^2} \tag{2.15}$$

Substitute t into (2.13), $\mathbf{P}_p$ can be calculated:

$$\mathbf{P}_p = \begin{bmatrix} x_{pp} \\ y_{pp} \\ z_{pp} \end{bmatrix} = \begin{bmatrix} x_{CC} + n_x \cdot r - \dfrac{n_x \cdot n_y \cdot \Delta y - n_y^2 \cdot \Delta x}{n_x^2 + n_y^2} \\ y_{CC} + n_y \cdot r + \dfrac{n_x^2 \cdot \Delta y - n_x \cdot n_y \cdot \Delta x}{n_x^2 + n_y^2} \\ z_{CC} + n_z \cdot r \end{bmatrix} \tag{2.116}$$

Substitute $\mathbf{P}_p$ into $\left|\overrightarrow{\mathbf{P}_p\mathbf{P}}\right| \geq r$,

$$\left[x - x_{CC} - n_x \cdot r + \frac{n_x \cdot n_y \cdot \Delta y - n_y^2 \cdot \Delta x}{n_x^2 + n_y^2}\right]^2 + \left[y - y_{CC} - n_y \cdot r - \frac{n_x^2 \cdot \Delta y - n_x \cdot n_y \cdot \Delta x}{n_x^2 + n_y^2}\right]^2 + \left[z - z_{CC} - n_z \cdot r\right]^2 \geq r^2 \tag{2.17}$$

Simplify the Ineq. (2.17), we have the first criterion,

$$\left(n_x^2 \cdot \Delta x + n_x \cdot n_y \cdot \Delta y\right)^2 + \left(n_y^2 \cdot \Delta y + n_x \cdot n_y \cdot \Delta x\right)^2 + \left(\Delta z / \lambda^2\right)^2 \geq \left(r / \lambda^2\right)^2 \tag{2.128}$$

Criterion two: **P** should be on the side of the plane $\mathbf{PL}_3$ where $\mathbf{P}_1$ locates.

Surface normal of $\mathbf{PL}_3$ is $\left[n_x, n_y, 0\right]^T$. From $\overrightarrow{\mathbf{P}_p\mathbf{P}} \cdot \left[n_x, n_y, 0\right]^T \leq 0$, we have,

$$\left(\begin{bmatrix} x \\ y \\ z \end{bmatrix} - \begin{bmatrix} x_{cc} + n_x \cdot r - \dfrac{n_x \cdot n_y \cdot y_{dif} - n_y^2 \cdot x_{dif}}{n_x^2 + n_y^2} \\ y_{cc} + n_y \cdot r + \dfrac{n_x^2 \cdot y_{dif} - n_x \cdot n_y \cdot x_{dif}}{n_x^2 + n_y^2} \\ z_{cc} + n_z \cdot r \end{bmatrix} \right) \cdot \begin{bmatrix} n_x \\ n_y \\ 0 \end{bmatrix} \le 0 \tag{2.139}$$

Simplify Ineq. (2.19), the second criterion can be obtained,

$$n_x \cdot \left(n_x^2 \cdot \Delta x + n_x \cdot n_y \cdot \Delta y \right) + n_y \cdot \left(n_y^2 \cdot \Delta y + n_x \cdot n_y \cdot \Delta x \right) \le 0 \tag{2.20}$$

So, when Eq. (2.18) and Eq. (2.20) exist, $R = \infty$.

- Case 3

Otherwise, a feasible imaginary cutter exists. Then we have the following equations,

$$\left[x - \left(x_{CC} + r \cdot n_x + R \cdot \lambda \cdot n_x \right) \right]^2 + \left[y - \left(y_{CC} + r \cdot n_y + R \cdot \lambda \cdot n_y \right) \right]^2 = \left(R + \sqrt{r^2 - \Delta z^2} \right)^2 \tag{2.21}$$

From Eq. (2.21),

$$R = \frac{\Delta x^2 + \Delta y^2 + \Delta z^2 - r^2}{2 \cdot \lambda \cdot n_x \cdot \Delta x + 2 \cdot \lambda \cdot n_y \cdot \Delta y + 2 \cdot \sqrt{r^2 - \Delta z^2}} \tag{2.22}$$

Condition 3: $\Delta z \le -r \cdot \cos\psi$

In this condition, **P** is below the plane $\mathbf{PL}_2$ as shown in Fig. 2-4. Only conical surface **CS** can touch **P**. There are three cases existing in terms of the location of the testing point **P**.

- Case 1

If **P** is in the volume bounded by $\mathbf{CS}_0$, **P** will be gouged undoubtedly. Then, R can be set as 0. The testing point **P** should satisfy the following inequality equations:

$$\Delta x^2 + \Delta y^2 \le \left(\frac{\Delta z + r \cdot \sec\psi}{\tan\psi} \right)^2 \tag{2.23}$$

and,

$$\Delta z > -r \cdot \sec\psi \tag{2.24}$$

- Case 2

In Fig. 2-3, if **P** locates below $\mathbf{CS}_\infty$, **P** will not be gouged. Then, R can be set as ∞. The surface normal of $\mathbf{CS}_\infty$ is $\overrightarrow{\mathbf{P}_2\mathbf{P}_0}$ and can be expressed as $\left[\lambda \cdot n_x \cdot \sin\psi, \lambda \cdot n_y \cdot \sin\psi, \cos\psi\right]^T$, so, **P** satisfies the following inequality equation if $R = \infty$:

$$\overrightarrow{\mathbf{P}_2\mathbf{P}} \cdot \overrightarrow{\mathbf{P}_2\mathbf{P}_0} \le 0 \tag{2.25}$$

Then, we have all satisfied testing points **P**,

$$\left(\begin{bmatrix} x \\ y \\ z \end{bmatrix} - \begin{bmatrix} x_{CC} + r \cdot n_x - r \cdot \lambda \cdot n_x \cdot \sin\psi \\ y_{CC} + r \cdot n_y - r \cdot \lambda \cdot n_y \cdot \sin\psi \\ z_{CC} + r \cdot n_z - r \cdot \cos\psi \end{bmatrix}\right) \cdot \begin{bmatrix} \lambda \cdot n_x \cdot \sin\psi \\ \lambda \cdot n_y \cdot \sin\psi \\ \cos\psi \end{bmatrix} \leq 0 \tag{2.26}$$

Ineq. (2.26) can be simplified as:

$$\lambda \cdot n_x \cdot \Delta x \cdot \sin\psi + \lambda \cdot n_y \cdot \Delta y \cdot \sin\psi + \Delta z \cdot \cos\psi + r \leq 0 \tag{2.147}$$

- Case 3

Otherwise, **P** is on the conical surface **CS** of a feasible imaginary cutter, we have the following equation:

$$\begin{aligned} &\left[x - \left(x_{CC} + r \cdot n_x + R \cdot \lambda \cdot n_x\right)\right]^2 + \left[y - \left(y_{CC} + r \cdot n_y + R \cdot \lambda \cdot n_y\right)\right]^2 \\ &= \left[\frac{z - \left(z_{CC} + n_z \cdot r - r \cdot \cos\psi\right)}{\tan\psi} + r \cdot \sin\psi + R\right]^2 \end{aligned} \tag{2.28}$$

Then we have,

$$\left(\Delta x - R \cdot \lambda \cdot n_x\right)^2 + \left(\Delta y - R \cdot \lambda \cdot n_y\right)^2 = \left(\frac{\Delta z + r \cdot \cos\psi}{\tan\psi} + r \cdot \sin\psi + R\right)^2 \tag{2.29}$$

Simplify the Eq. (2.29),

$$R = \frac{\Delta x^2 + \Delta y^2 - \left(\frac{\Delta z}{\tan\psi} + 2 \cdot r \cdot \sin\psi\right)^2}{2 \cdot \Delta x \cdot \lambda \cdot n_x + 2 \cdot \Delta y \cdot \lambda \cdot n_y + 2 \cdot \left(\frac{\Delta z}{\tan\psi} + 2 \cdot r \cdot \sin\psi\right)} \tag{2.30}$$

2.3.3 Imaginary cutter size model for the tapered ball end-mills

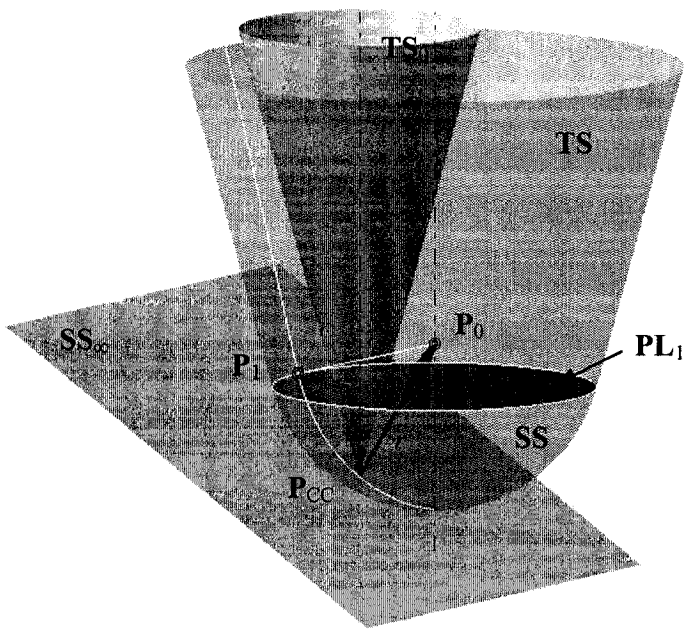

Figure 2-5: Example of an imaginary ball end-mill and its two extreme case: R=0 or R=∞.

Because tapered ball end-mill use r as a variable, here, we treat tapered ball end-mill as a special case of general APT cutter. Fig. 2-5 shows an imaginary ball end-mill and its two extreme cases. The cutting envelop of a feasible imaginary cutter comprises two portions: a tapered surface (**TS**), and a spherical surface (**SS**). These portions will shrink to $\mathbf{TS}_0$ or extend to $\mathbf{SS}_\infty$ when R equals zero or infinite large. The cutting envelop of every feasible imaginary cutter is inside the volume bounded by $\mathbf{TS}_0$ and $\mathbf{SS}_\infty$. Then, if a testing point **P** is outside this volume, there is no feasible imaginary cutter existing, however, if the testing point **P** is inside this volume, a feasible

imaginary cutter can always be found. To judge which portion of the cutting envelop will touch the testing point **P**, $\mathbf{PL}_1$ are used and shown in Fig. 2-4. $\mathbf{PL}_1$ is the plane on which the intersection circle between **TS** and **SS** locates. If **P** is above $\mathbf{PL}_1$, only the tapered surface has chance to touch **P**. If **P** is below $\mathbf{PL}_1$, only the spherical surface can pass **P**. Then, the imaginary cutter size can be calculated through the following equations.

Condition 1

$\mathbf{SS}_\infty$ is a plane which is passing through $\mathbf{P}_{CC}$ and perpendicular with the surface normal $\mathbf{N}_{CC}$. Hence, if **P** is below the $\mathbf{SS}_\infty$, no matter how large the cutter radius r is, the tapered ball end-mill cannot touch **P**. In this case, $r = \infty$. This criterion can be written as:

$$\left(\begin{bmatrix} x \\ y \\ z \end{bmatrix} - \begin{bmatrix} x_{CC} \\ y_{CC} \\ z_{CC} \end{bmatrix}\right) \cdot \begin{bmatrix} n_x \\ n_y \\ n_z \end{bmatrix} \le 0 \tag{2.31}$$

Simplify Eq. (2.31), we get

$$n_x \cdot (x - x_{CC}) + n_y \cdot (y - y_{CC}) + n_z \cdot (z - z_{CC}) \le 0 \tag{2.32}$$

Condition 2

When the cutter radius r is zero (see Fig. 2-5), the envelope of a ball end-mill becomes a conical surface $\mathbf{TS}_0$. Any test point **P** located in the volume bounded by $\mathbf{TS}_0$ will result in gouging. This criterion can be written as follows,

$$\frac{\sqrt{(x-x_{CC})^2+(y-y_{CC})^2}}{z-z_{CC}} \le \tan\theta \tag{2.33}$$

If **P** satisfies the Ineq. (2.33), cutter radius r can be set as 0.

- Condition 3

If **P** does not satisfy Ineq (2.32) and (2.32), A feasible imaginary tapered ball end-mill exists and can machine $\mathbf{P}_{CC}$ and at the same time touch **P**.

We have following cases:

- Case 1, $z \le z_{CC}$

In this case, **P** can only be touched by the spherical portion **SS** of the cutting surface. The distance between **P** and the center point $\mathbf{P}_0$ of the spherical surface is always the cutter radius. Then the following equation exists:

$$\left[x-\left(x_{CC}+r\cdot n_x\right)\right]^2+\left[y-\left(y_{CC}+r\cdot n_y\right)\right]^2+\left[z-\left(z_{CC}+r\cdot n_z\right)\right]^2=r^2 \tag{2.34}$$

From Eq. (2.33), the cutter size can be obtained:

$$r = \frac{1}{2} \cdot \frac{(x - x_{CC})^2 + (y - y_{CC})^2 + (z - z_{CC})^2}{n_x \cdot (x - x_{CC}) + n_y \cdot (y - y_{CC}) + n_z \cdot (z - z_{CC})} \tag{2.35}$$

- Case 2, $z > z_{CC}$

In this case, the testing point **P** can be either on the spherical surface **SS** or on the tapered surface **TS**. To determination that, the reference radius is introduced as follows:

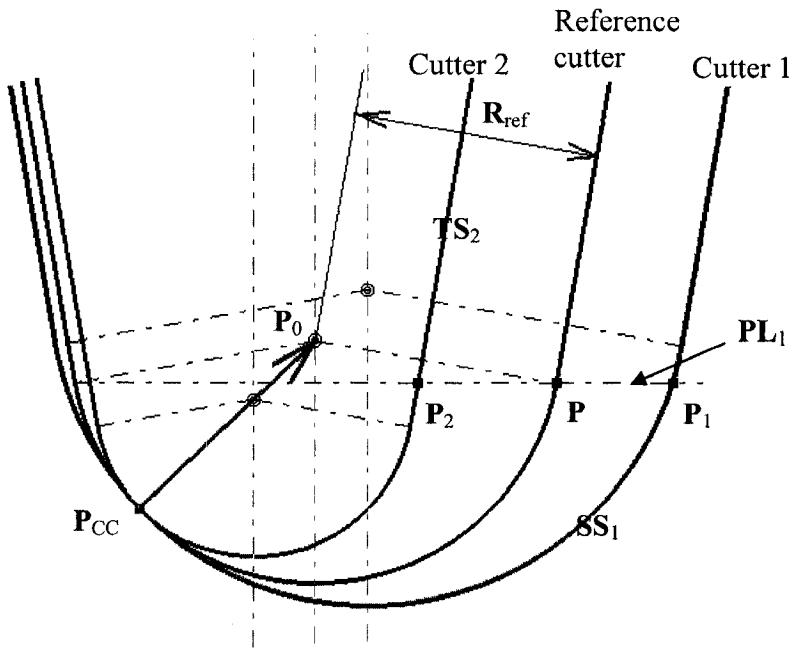

Figure 2-6: Model of reference cutters

In Fig. 2-6, with the increase of cutter radius r, $\mathbf{PL}_1$ is rising too. Once the $\mathbf{PL}_1$ passes through **P**, the cutter radius of this reference cutter is reference radius (R_{ref}). The following equation can be generated:

$$z_{CC} + n_z \cdot R_{ref} - \sin\theta \cdot R_{ref} = z \tag{2.36}$$

From Eq. (2.36), R_{ref} can be obtained:

$$R_{ref} = \frac{z - z_{CC}}{n_z - \sin\theta} \tag{2.37}$$

Then the cutter radius r can be determined as follows:

If $(x - x_{CC} - n_x \cdot R_{ref})^2 + (y - y_{CC} - n_y \cdot R_{ref})^2 > (R_{ref} \cdot \cos\theta)^2$, the testing point is outside the reference cutter, as $\mathbf{P}_1$ shown in Fig. 2-6. The reference cutter should be enlarged to cutter 1, whose cutting surface touches $\mathbf{P}_1$. With increase of r, the level of $\mathbf{PL}_1$ will rise. So, only spherical surface $\mathbf{SS}_1$ has the chance to touch $\mathbf{P}_1$. Cutter radius r then can be obtained from Eq. (2.34).

If $(x - x_{CC} - n_x \cdot R_{ref})^2 + (y - y_{CC} - n_y \cdot R_{ref})^2 = (R_{ref} \cdot \cos\theta)^2$, then, the testing point is on the cutting surface of the tapered ball end-mill, $r = R_{ref}$, as $\mathbf{P}_2$ shown in Fig. 2-6.

If $(x - x_{CC} - n_x \cdot R_{ref})^2 + (y - y_{CC} - n_y \cdot R_{ref})^2 < (R_{ref} \cdot \cos\theta)^2$, the testing point is inside the cutter, as $\mathbf{P}_2$ shown in Fig. 2-6. The reference cutter radius should shrink to cutter 2, whose cutting surface touches **P**. When r decreases, the level of $\mathbf{PL}_1$ will decline. So, only tapered surface $\mathbf{TS}_2$ can touch $\mathbf{P}_2$. The following equation exists:

$$\left[x-\left(x_{CC}+r\cdot n_x\right)\right]^2+\left[y-\left(y_{CC}+r\cdot n_y\right)\right]^2=\left\{\left[z-\left(z_{CC}+r\cdot n_z\right)\right]\cdot\tan\theta+r\cdot\sec\theta\right\}^2 \quad (2.38)$$

From Eq. (2.38), we have:

$$\begin{aligned}&\left(x-x_{CC}\right)^2-2\cdot\left(x-x_{CC}\right)\cdot n_x\cdot r+n_x^2\cdot r^2+\left(y-y_{CC}\right)^2-2\cdot\left(y-y_{CC}\right)\cdot n_y\cdot r+n_y^2\cdot r^2=\\&\left(\sec\theta-n_z\cdot\tan\theta\right)^2\cdot r^2+2\cdot\left(z-z_{CC}\right)\cdot\tan\theta\cdot\left(\sec\theta-n_z\cdot\tan\theta\right)\cdot r+\left(z-z_{CC}\right)^2\cdot\tan^2\theta\end{aligned} \quad (2.39)$$

Then we have,

$$e_1\cdot r^2+e_2\cdot r+e_3=0 \quad (2.40)$$

$$r=\frac{-e_2+\sqrt{e_2^2-4\cdot e_1\cdot e_3}}{2\cdot e_1} \quad (2.41)$$

Here,

$$e_1=\left(\sec\theta-n_z\cdot\tan\theta\right)^2-n_x^2-n_y^2 \quad (2.42)$$

$$e_2=2\cdot\left(z-z_{CC}\right)\cdot\tan\theta\cdot\left(\sec\theta-n_z\cdot\tan\theta\right)+2\cdot n_x\cdot\left(x-x_{CC}\right)+2\cdot n_y\cdot\left(y-y_{CC}\right) \quad (2.43)$$

$$e_3=\left(z-z_{CC}\right)^2\cdot\tan^2\theta-\left(x-x_{CC}\right)^2-\left(y-y_{CC}\right)^2 \quad (2.44)$$

There is a special case: when $n_z=\sin\theta$, we have $e_1=0$, r can be obtained from Eq. (2.40):

$$r=-\frac{e_3}{e_2}=\frac{\left(x-x_{CC}\right)^2+\left(y-y_{CC}\right)^2-\left(z-z_{CC}\right)^2\cdot\tan^2\theta}{2\cdot\left(z-z_{CC}\right)\cdot\sin\theta+2\cdot n_x\cdot\left(x-x_{CC}\right)+2\cdot n_y\cdot\left(y-y_{CC}\right)} \quad (2.45)$$

2.3.4 Algorithm of the allowable cutter size determination at a CC point

A computer program can be established in terms of the cutter type, known cutter parameters and surface information. Allowable cutter size determination procedure can be performed by using the following algorithm.

1) Determine the cutter type, if it is a ball end-mill, go to 13.

2) If $\Delta z \geq -r \cdot \sin\theta$, otherwise go to 6.

3) If $\Delta x^2 + \Delta y^2 \leq (\Delta z \cdot \tan\theta + r \cdot \sec\theta)^2$, $R = 0$, go to 21.

4) If $\lambda \cdot n_x \cdot \Delta x \cdot \cos\theta + \lambda \cdot n_y \cdot \Delta y \cdot \cos\theta + \Delta z \cdot \sin\theta + r \leq 0$, $R = \infty$, go to 21.

5) $R = \frac{1}{2} \cdot \frac{\Delta x^2 + \Delta y^2 - (\Delta z \cdot \tan\theta + r \cdot \sec\theta)^2}{\lambda \cdot n_x \cdot \Delta x + \lambda \cdot n_y \cdot \Delta y + \Delta z \cdot \tan\theta + r \cdot \sec\theta}$, go to 21.

6) If $-r \cdot \cos\psi < \Delta z < -r \cdot \sin\theta$, otherwise go to 10.

7) If $\Delta x^2 + \Delta y^2 + \Delta z^2 \leq r^2$, $R = 0$, go to 21.

8) If $\left(n_x^2 \cdot \Delta x + n_x \cdot n_y \cdot \Delta y\right)^2 + \left(n_y^2 \cdot \Delta y + n_x \cdot n_y \cdot \Delta x\right)^2 + \left(\Delta z / \lambda^2\right)^2 \geq \left(r / \lambda^2\right)^2$ and

$n_x \cdot \left(n_x^2 \cdot \Delta x + n_x \cdot n_y \cdot \Delta y\right) + n_y \cdot \left(n_y^2 \cdot \Delta y + n_x \cdot n_y \cdot \Delta x\right) \leq 0$, $R = \infty$, go to 21.

9) $R = \frac{\Delta x^2 + \Delta y^2 + \Delta z^2 - r^2}{2 \cdot \lambda \cdot n_x \cdot \Delta x + 2 \cdot \lambda \cdot n_y \cdot \Delta y + 2 \cdot \sqrt{r^2 - \Delta z^2}}$, go to 21.

10) If $\lambda \cdot n_x \cdot \Delta x \cdot \sin\psi + \lambda \cdot n_y \cdot \Delta y \cdot \sin\psi + \Delta z \cdot \cos\psi + r \leq 0$, $R = \infty$, go to 21.

11) If $x^2 + y^2 \leq \left(\frac{z + r \cdot \sec\psi}{\tan\psi}\right)^2$, $R = 0$, go to 21.

12) $R = \dfrac{\Delta x^2 + \Delta y^2 - \left(\dfrac{\Delta z}{\tan\psi} + 2\cdot r\cdot\sin\psi\right)^2}{2\cdot\Delta x\cdot\lambda\cdot n_x + 2\cdot\Delta y\cdot\lambda\cdot n_y + 2\cdot\left(\dfrac{\Delta z}{\tan\psi} + 2\cdot r\cdot\sin\psi\right)}$, go to 21.

13) If $n_x\cdot(x - x_{CC}) + n_y\cdot(y - y_{CC}) + n_z\cdot(z - z_{CC}) \le 0$, $r = \infty$, go to 21.

14) If $\dfrac{\sqrt{(x - x_{CC})^2 + (y - y_{CC})^2}}{z - z_{CC}} \le \tan\theta$, $r = 0$, go to 21.

15) If $z \le z_{CC}$, $r = \dfrac{1}{2}\cdot\dfrac{(x - x_{CC})^2 + (y - y_{CC})^2 + (z - z_{CC})^2}{n_x\cdot(x - x_{CC}) + n_y\cdot(y - y_{CC}) + n_z\cdot(z - z_{CC})}$, go to 21

16) If $n_z = \sin\theta$, $r = \dfrac{(x - x_{CC})^2 + (y - y_{CC})^2 - (z - z_{CC})^2\cdot\tan^2\theta}{2\cdot(z - z_{CC})\cdot\sin\theta + 2\cdot n_x\cdot(x - x_{CC}) + 2\cdot n_y\cdot(y - y_{CC})}$, go to 21.

17) Calculate $R_{ref} = \dfrac{z - z_{CC}}{n_z - \sin\theta}$,

18) If $(x - x_{CC} - n_x\cdot R_{ref})^2 + (y - y_{CC} - n_y\cdot R_{ref})^2 > (R_{ref}\cdot\cos\theta)^2$,

$r = \dfrac{1}{2}\cdot\dfrac{(x - x_{CC})^2 + (y - y_{CC})^2 + (z - z_{CC})^2}{n_x\cdot(x - x_{CC}) + n_y\cdot(y - y_{CC}) + n_z\cdot(z - z_{CC})}$, go to 21.

19) If $(x - x_{CC} - n_x\cdot R_{ref})^2 + (y - y_{CC} - n_y\cdot R_{ref})^2 = (R_{ref}\cdot\cos\theta)^2$, $r = R_{ref}$, go to 21.

20) If $(x - x_{CC} - n_x\cdot R_{ref})^2 + (y - y_{CC} - n_y\cdot R_{ref})^2 < (R_{ref}\cdot\cos\theta)^2$, $r = \dfrac{-e_2 + \sqrt{e_2^2 - 4\cdot e_1\cdot e_3}}{2\cdot e_1}$, go to 21.

Here,

$e_1 = (\sec\theta - n_z\cdot\tan\theta)^2 - n_x^2 - n_y^2$

$e_2 = 2\cdot(z - z_{CC})\cdot\tan\theta\cdot(\sec\theta - n_z\cdot\tan\theta) + 2\cdot n_x\cdot(x - x_{CC}) + 2\cdot n_y\cdot(y - y_{CC})$

$$e_3 = (z - z_{CC})^2 \cdot \tan^2\theta - (x - x_{CC})^2 - (y - y_{CC})^2$$

21) END of calculation, output imaginary cutter size R_{CC}, which is R for the flat end-mill & bull-nose end-mill or r for the ball end-mill.

2.4 Optimization problem of the allowable cutter size at a CC point

2.4.1 The allowable cutter size at a CC point for 3-axis sculptured surface machining

In theory, to machine a compound surface at a CC point in the most efficient way, a cutter in allowable size is needed, which touches the component surfaces at discrete points without intersecting with them. This allowable cutter size can be found by testing every point on the compound surface and calculating the radius of its corresponding imaginary cutter with the above-mentioned equations. If the radius is infinite, no cutter can gouge the surface at the testing point when machining the CC point. This point thus does not determine the allowable cutter size. Generally, the cutting surface of the calculated cutter passes through the testing point while contacting the compound surface at the CC point; however, it also intersects with the compound surface, over-cutting it. Although this cutter is not in the allowable size, it is easy to understand that if we test all the points across the compound surface, the cutter size will gradually decrease on the whole, and the intersection between the cutter and this surface will be reduced accordingly. Until, at one testing point, the cutter size drops to the minimum, and the intersection converges to this point. Since this imaginary cutter is the largest without gouging and interference, its radius is the

allowable cutter size. For an extreme case, if $R_{CC}(\mathbf{P})$ is zero, the CC point cannot be accessed with any APT cutter without gouging; therefore it cannot be machined.

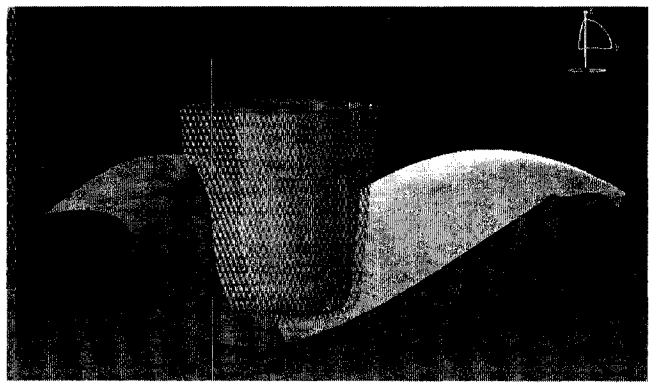

Figure 2-7: Example of imaginary cutter and allowable cutter

It is evident that the allowable cutter size for a CC point can be found by minimizing an imaginary cutter radius through testing all the points on the compound surface. Therefore, the allowable cutter size at a CC point can be formulated as follows. For any testing point on the compound surface $\mathbf{P} \in \mathbf{S}$, the radius of its corresponding imaginary cutter can be computed as $R_{CC}(\mathbf{P})$, if an APT cutter is to cut the CC point $\mathbf{P}_{CC}$, and $r_{CC}(\mathbf{P})$, if a ball end-mill is to be used. Since by searching all the points $\mathbf{P}$, the cutter radius can be minimized, the allowable cutter size is the solution of the global optimization problem, which the objective function is $R_{CC}(\mathbf{P})$ or $r_{CC}(\mathbf{P})$,

$$\text{minimize: } \begin{cases} R_{cc}^{*} = R_{CC}\left[\mathbf{P}(u,v)\right], & \text{if an APT cutter is used} \\ r_{cc}^{*} = r_{CC}\left[\mathbf{P}(u,v)\right], & \text{if a ball end-mill is used} \end{cases};$$

$$\text{subject to: } \begin{cases} \mathbf{P}(u,v) \in \mathbf{S}, \ (u,v) \in \Re^2 \\ \mathbf{P} \neq \mathbf{P}_{CC} \end{cases}$$

2.4.2 The largest allowable cutter size and the cutter orientation at a CC point for 4-axis sculptured surface machining

For 4-axis sculptured surface machining, to establish the cutter model for the largest allowable cutter size based on the above-mentioned theorem, first, assume a part with sculptured surfaces, such as an axial-flow compressor, is set up on the rotary table with angle B in 4-axis CNC milling. By changing angle B, the size of the open space for the cutter to access CC points on the blade surface is changed accordingly. Thus, for each CC point, the allowable cutter size is a function of angle B; given an angle B, the allowable cutter size can be found using the method introduced above. At an optimum angle $B_{\max}$, the allowable cutter reaches the maximum size. The equation for this largest allowable cutter size is formulated.

$$\begin{aligned} & R_{\max} = \max\left[R_{allowable}(B)\right] = \max\left\{\min\left[R_{CC}(\mathbf{P}, B)\right]\right\} \\ & \text{Subject to: } 360^{\circ} \geq B \geq 0^{\circ} \\ & \qquad \mathbf{P} \in \mathbf{S}_i \ (i = 0, 1, 2, \ldots, n) \end{aligned} \tag{2.2}$$

Again, apply the optimization method to find the optimum angle $B_{\max}$ and the maximum allowable cutter size $R_{\max}$ for this CC point. In CNC machining, when the angle is equal to $B_{\max}$, the open space for the cutter is the largest, so it is safe to cut

this CC point without gouging and interference by using a cutter that is smaller than the maximum allowable cutter in this orientation.

To solve this problem, a hybrid optimization method, the integration of the particle swarm optimization (PSO) and local optimization methods, is employed. This new method has taken the advantages of both the global optimization method and the local optimization method, thus, it can effectively find the minimum solution for the allowable cutter size.

Chapter 3 Hybrid Global Optimization Method

3.1 Global optimization problems

The above-mentioned model of the allowable cutter size at a CC point is a global optimization problem due to the high non-linearity of the sculptured surface patches of a compound surface. To illustrate the global feature of this problem, two typical surfaces $\mathbf{S}_1$ and $\mathbf{S}_2$ are employed (Fig. 3-1). At a fixed CC point $\mathbf{P}_{CC}$ $\left([u,v]=[0.45,0.725]\right)$ on the surface $\mathbf{S}_1$, any point $\mathbf{P}$ on the surface $\mathbf{S}_2$ determines the radius of an imaginary cutter.

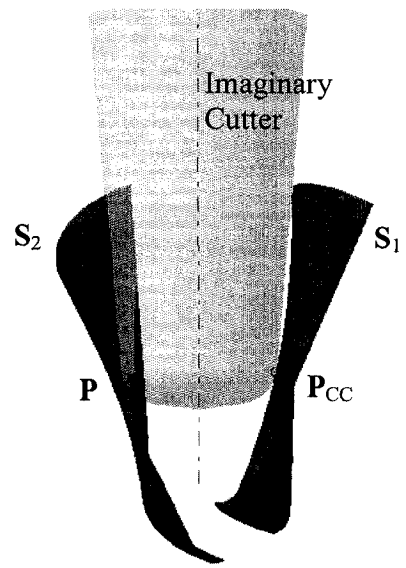

Figure 3-1: Example of a global optimization problem

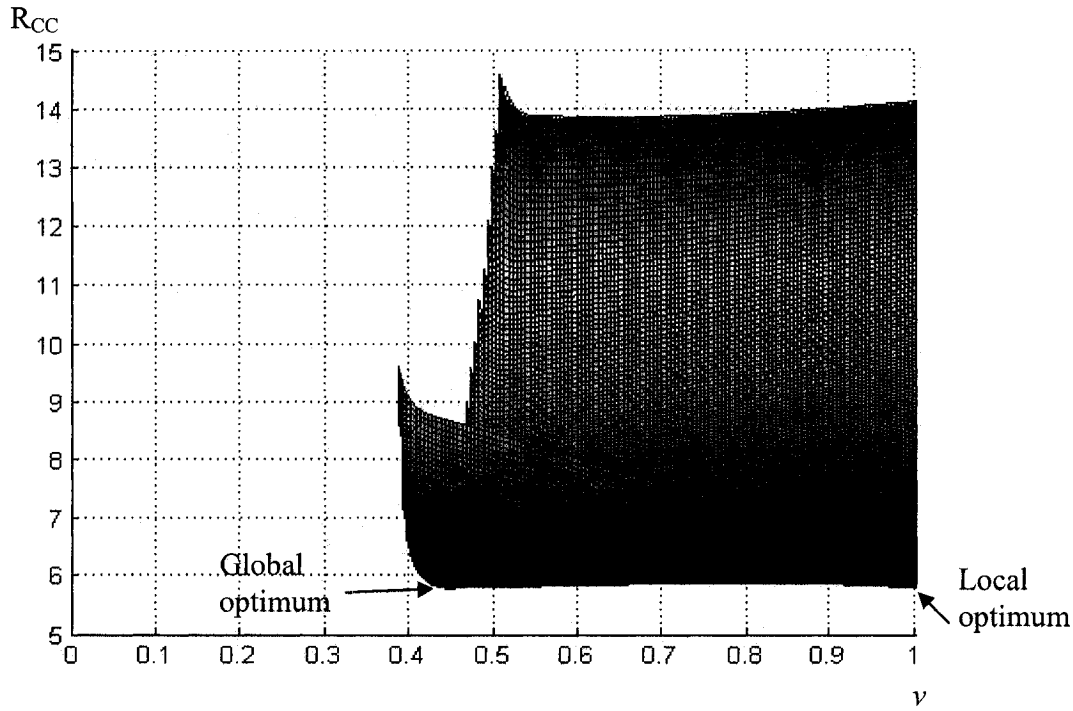

Figure 3-2: Imaginary cutter radii map

When **P** changes in the domain $(u \in [0,1], v \in [0,1])$ of $\mathbf{S}_2$, the imaginary cutter radius will change accordingly; thus, a radii map of all the imaginary cutters is plotted in Fig. 3-2. In this figure, the saddle shape on the map indicates that there are a local and a global minimum values of the imaginary cutters; the global minimum value is 5.8139 mm at point $\mathbf{P}([u,v]=[0.34,0.45])$ and the local optimum is 5.8186 mm at point $\mathbf{P}([u,v]=[0.15,1.0])$. Therefore, it is readily to see that the model of allowable cutter size is a global optimization problem.

The genetic algorithm, simulated annealing, and particle swarm optimization (PSO) methods are commonly used global optimization methods to solve the global

optimization problems. Since these solutions employ stochastic technique, normally, they require a great number of iterations and converge slowly, especially in the neighbourhood of the global optimum. The well-established local optimization methods are quick to converge at a local solution; however, they could not find the global solution. To take the advantages of both methods and overcome their drawbacks, in this work, a hybrid method is proposed, which, first, employs the PSO method to search for the local solution region where global optimum locates, and then apply the local optimization method to find the global optimum.

3.2 Introduction to the particle swarm optimization method

The current PSO method is featured with population-based search by imitating a swarm of scattered particles exploring the problem domain, in order to find the global solution to a complicated optimization problem. In this method, first, a swarm of particles are scattered around in the problem domain, and then a search process begins. In the iteration of this search, these particles move in randomly-determined velocities to explore the objective function at different locations (or possible solutions) for its minimum. To ensure each particle moving along a correct direction in a step, its best location (the value of the objective function at this location is less than those at all its previous locations) is updated; so is the swarm's best location (the value of the objective function at this location is less than those at the locations all the particles have visited before). After the searching results are stable, the local area of the solution is identified.

In this work, the objective function $R_{CC}[\mathbf{P}(u,v)]$ is in the compound surface domain $\Re^2$, if an APT cutter is used, and the constraint is that all points $\mathbf{P}(u,v)$ are on the compound surface and are not the CC point. The PSO method is adopted to solve this problem. First, n particle points $\left(\mathbf{P}_1(u_1,v_1),\ \mathbf{P}_2(u_2,v_2),\ ...,\ \mathbf{P}_j(u_j,v_j),\ ...,\ \mathbf{P}_n(u_n,v_n)\right)$ are randomly chosen on the compound surface $\left(\mathbf{P}_j \in \mathbf{S},\ (u_j,v_j) \in \Re^2\right)$. The maximal parametric displacement for all particle points is specified as $[\Delta u_{max},\ \Delta v_{max}]$. Generally, the location and displacement of particle point $\mathbf{P}_j$ in iteration t are represented as $[u_j(t),\ v_j(t)]$ and $[\Delta u_j(t),\ \Delta v_j(t)]$, respectively. All particles' best locations are $[\hat{u}_j,\ \hat{v}_j]$, $(j=1,\ 2,\ ...,\ n)$, and the swarm's best location is $[u_{best},\ v_{best}]$ are constantly updated in the searching process. Based on their values in iteration (t), the velocity and position of particle i can be calculated for the next iteration $(t+1)$, according to the following recursive equations.

$$\begin{cases} \Delta u_j(t+1) = c_1 \cdot u_j(t) + c_2 \cdot \text{rand}(\ ) \cdot [\hat{u}_j - u_j(t)] + c_3 \cdot \text{rand}(\ ) \cdot [u_{best} - u_j(t)] \\ u_j(t+1) = u_j(t) + \min[\Delta u_j(t+1),\ \Delta u_{max}] \end{cases} \tag{3.1}$$

and

$$\begin{cases} \Delta v_j(t+1) = c_1 \cdot v_j(t) + c_2 \cdot \text{rand}(\ ) \cdot [\hat{v}_j - v_j(t)] + c_3 \cdot \text{rand}(\ ) \cdot [v_{best} - v_j(t)] \\ v_j(t+1) = v_j(t) + \min[\Delta v_j(t+1),\ \Delta v_{max}] \end{cases} \tag{3.2}$$

where c_1 is an inertia weight, c_2 and c_3 are acceleration coefficients, and rand( ) is the uniform distribution function that generates random numbers between 0 and 1. These equations are applied to all particles for their new locations.

After the particles reach the new positions, the objective function is evaluated for each particle. The particles' best positions and the swarm's best position are updated based on the following criteria. If

$$R_{CC}\left[\mathbf{P}_j\left(u_j(t), v_j(t)\right)\right] > R_{CC}\left[\mathbf{P}_j\left(u_j(t+1), v_j(t+1)\right)\right] \tag{3.3}$$

then $\left[\hat{u}_j, \hat{v}_j\right] = \left[u_j(t+1), v_j(t+1)\right]$, $(j = 1,\ 2,\ ...,\ \mathrm{n})$. If

$$R_{CC}\left[P_{j^*}\left(u_{j^*}(t+1), v_{j^*}(t+1)\right)\right] < \min\left\{R_{CC}\left[\mathbf{P}(u_{best}, v_{best})\right], R_{CC}\left[P_j\left(u_j(t+1), v_j(t+1)\right)\right]\right\}$$

$j^* \in [1,\ 2,\ ...,\ \mathrm{n}]$, and $j = 1,\ 2,\ ...,\ \mathrm{n}$, then

$$\left[u_{best},\ v_{best}\right] = \left[u_{j^*}(t+1),\ v_{j^*}(t+1)\right]$$

With Ineq. (3.3), the PSO method collects the cognitive information at the particles' best positions and the social information at the swarm's best position. When the iteration number exceeds the specified value or the function value at the swarm's best position converges, the search stops, and this position is output as the solution to the problem.

The population size, the inertia weight, and the acceleration coefficients are crucial to the efficiency and convergence of the PSO method; however, these parameters are dependent on different problems, and there is no fixed rule for them. In general, these parameters are assigned with the values listed in Tab. 3-1. In my research, extensive tests will be conducted in order to find proper values for the parameters.

Table 3-1: Popular values for the parameters of the PSO method

Repeat number	Population size	Inertia weight	c_2	c_3
30	50 - 100	$[0.1, 0.2]$	0.5	0.5

3.3 Hybrid optimization method

Incorporating a local search strategy into a global optimization method can be done in various ways. One of hybridization techniques follows the so-called Lamarckian approach [30] in which the local search algorithm is applied to some newly generated individuals to drive them to a local optimum. These locally optimal solutions replace the current individuals in the population to prepare the next generation. However, this hybridization technique is unnecessary and time consuming. In this study, the hybridization technique follows two steps to reach the global optimal value. First, PSO is implemented until it terminates and then a conventional optimization method is applied to obtain the final solution. The criteria to terminate PSO are set in the way that the global search ability of PSO is enhanced in terms of some tests which had been done before programming. Particle number, repeat number, inertia weight and acceleration

coefficients are carefully selected to encourage particles to move more effectively and efficiently to find the possible range where global optimum locates.

To find proper values for the parameters of the PSO method in my research, the example of cutting the CC point $\mathbf{P}_{CC}$ on surface $\mathbf{S}_1$, shown in Fig. 3-1, is adopted. Since the difference between the local minimum radius (5.8186 mm) and the global minimum radius (5.8139 mm) is very small (0.0047 mm), the PSO method could easily miss the global solution, if its parameters are not specified with appropriate values. Hence, to find these parameters' value, eight sets of values are specified; and each set is used in the PSO method to calculate the radius of the allowable cutter at the CC point 20 times. The typical computational results in the 20 tests by using one set of parameters are shown in Tab. 3-2, and Tab. 3-3 highlights the set of parameters with the best results, compared to all the results collected. In these tables, N_R is the prescribed number for repetitions, which means if the computed radius remains the same in N_R iterations, the search will be terminated. N_p is the population size of particles. N_a refers to the actual iteration number in each computation; N_1 is the iteration number, after which the calculated cutter radius deviates from the calculated allowable cutter radius by 0.001 mm; N_2 is the iteration number, after which the calculated cutter radius is less than the local minimum value of the allowable cutter size (5.8186 mm).

Table 3-2: The typical computation results using a set of specified values in the PSO method

Parameters set in PSO:
Repeat iteration number: $N_R = 100$
Population size: $N_P = 64$
Inertia weight: $c_1 \in [0.4, 0.9]$
Acceleration coefficients: $c_2 = c_3 = 2.0$

Test No.	N_a	Radius of allowable cutter (mm)	N_1	N_2
1	542	5.8133	42	15
2	530	5.8133	38	14
3	570	5.8133	8	6
4	617	5.8133	44	18
5	397	5.8186	9	
6	244	5.8135	144	121
7	754	5.8133	371	276
8	425	5.8186	7	
9	561	5.8133	5	5
10	146	5.8134	12	1
11	121	5.8134	5	5
12	131	5.8134	11	11
13	601	5.8133	72	12
14	553	5.8133	60	3
15	660	5.8133	206	182
16	528	5.8186	6	
17	145	5.8134	39	7
18	707	5.8133	27	10
19	682	5.8133	70	27
20	656	5.8133	246	166

Tab. 3-2 lists the set of parameters specified as $N_R(100)$, $N_P(64)$, $c_1 \in [0.4, 0.9]$, $c_2 = c_3 = 2.0$. In the first test, the PSO method has found the minimum cutter radius as 5.1833 mm after 542 iterations, while an imaginary cutter calculated in the 42th iteration is very close to the final result (within 0.001 mm). These results have verified that the PSO method can quickly identify the local region around the solution, but it would spend a long time to pinpoint the solution. Since the imaginary cutter in the 15th iteration is smaller than the local minimum cutter, the PSO method can search into the local region, where the global optimum lies, after 15 iterations. In this hybrid method, the PSO method is used to find this local region, and a gradient optimization method is then employed.

Compared the results in Tab. 3-2, the results in Tab. 3-3 demonstrate more computation efficiency by using a set of parameters, $N_R(30)$, $N_P(64)$, $c_1 \in [0.1, 0.2]$, $c_2 = c_3 = 0.5$. Thus, this set of parameters is adopted in the PSO method to solve the optimization problems in my research.

Table 3-3: Test of PSO parameter which has the best global search ability

Parameters set in PSO:
Repeat number: $N_R = 30$
Population size: $N_P = 64$
Inertia weight: $c_1 \in [0.1, 0.2]$
Acceleration coefficients: $c_2 = c_3 = 0.5$

Test No.	N_a	Radius of allowable cutter (mm)	N_1	N_2
1	92	5.8133	7	4
2	130	5.8133	8	7
3	272	5.8161	141	6
4	104	5.8133	4	4
5	194	5.8166	51	49
6	103	5.8133	7	6
7	187	5.8133	7	3
8	175	5.8152	71	70
9	112	5.8288	13	5
10	188	5.8157	77	5
11	96	5.8133	8	3
12	127	5.8134	27	9
13	110	5.8138	9	5
14	136	5.8135	9	3
15	116	5.8133	6	3
16	96	5.8133	4	1
17	174	5.8133	9	5
18	201	5.8133	7	3
19	111	5.8133	10	10
20	183	5.8183	74	40

Tab. 3-4 lists all the eight sets of specified values and the testing results by using them in the PSO method. In Tab. 3-4, percentage means the possibility of finding the global optimum region.

Table 3-4: Eight sets of parameters and the testing results

	1	2	3	4	5	6	7	8
N_R	100	10	10	10	20	20	30	30
N_P	64	64	64	100	100	100	64	64
c_1	[0.4, 0.9]	[0.4, 0.9]	[0.4, 0.9]	[0.4, 0.9]	[0.4, 0.9]	[0.1, 0.2]	[0.1, 0.2]	[0.4, 0.9]
c_2	2.0	2.0	0.5	0.5	0.5	0.5	0.5	0.5
c_3	2.0	2.0	0.5	0.5	0.5	0.5	0.5	0.5
$Max(N_a)$	707	61	47	49	239	214	272	287
$Min(N_a)$	121	20	12	17	23	56	96	43
$Ave(N_a)$	479	34	31	35	116	105	145	197
$Max(N_1)$	371	30	20	20	19	22	77	72
$Min(N_1)$	5	3	2	5	1	3	4	2
$Ave(N_1)$	71	11	12	12	12	8	28	14
$Max(N_2)$	276	29	14	15	10	9	49	11
$Min(N_2)$	1	4	1	3	1	2	1	2
Percentage	85	55	85	65	70	80	100	70

From Tab. 3-2, Tab. 3-3 and Tab. 3-4, we can conclude:

- As a stochastic method, the PSO method often converges at the final result after a great number of iterations, while it can quickly find out a candidate that is very close to the optimum solution.
- Through adjusting the parameter values, the possibility to find out the global solution has been increased and the computation time remains in the average level.
- The hybrid optimization method is used in this research to achieve high computing efficiency and accuracy.

For this research work, medium-scale gradient algorithms in the optimization toolbox of MATLAB are used. Because there is no constrain in this problem, Nelder-Mead simplex search method and the BFGS (Broyden, Fletcher, Goldfarb, and Shanno) Quasi-Newton method are two local optimization methods which are used to solve this local optimization problem after the PSO method has searched into the local region where the solution lies in.

Chapter 4 Application: 3-Axis CNC Milling of Compound Surface Parts

4.1 Introduction

In the computer-aided mechanical design of aircrafts, automobiles, and dies/molds, compound surfaces are widely employed for complex shapes or details; each of these surfaces consists of several free-form surface patches connected with C^1 or C^2 continuity. In the process planning for the 3-axis finish machining of these surfaces, the cutters are always expected to be as large as possible for high productivity, but the cutters should not gouge the surfaces. Thus, the technique of determining the maximum allowable cutter sizes for compound surface finish machining is urgently needed in the manufacturing industry. However, due to the geometric complexity of a compound surface part, it is difficult to determine, according to the machinists' experience, the appropriate sizes for the cutters so that their shapes always match the part's surface at the cutter-contact (CC) points. Moreover, when the part is set up differently on a CNC machine tool, the appropriate cutter sizes for these set-ups can be quite different in machining. Unfortunately, the cutter size determination for compound surface machining has not yet been satisfactorily addressed.

To determine cutter sizes for 3-axis milling of compound surfaces, the factors such as gouging and interference avoidance and standard cutters available in industry should be taken into consideration. In this research, a new, practical approach is proposed to determine the maximum cutter sizes without gouging the compound surfaces. First, this research is mainly focused on computing the allowable cutter size without gouging and interference at one cutter-contact (CC) point, by applying the imaginary cutter radius algorithms on all the compound surfaces. Second, the allowable cutter sizes for all CC points are calculated and an allowable cutter radius map can be created for selection of cutters. Then, based on the available standard cutters, the sizes of several cutters can be decided for the 3-axis machining of the whole compound surface. Finally, hair dryer mold example is provided to verify this proposed study.

4.2 Selection of appropriate standard cutters for the compound surface machining

In industry, in order to efficiently cut compound surfaces on 3-axis CNC machines, several appropriate standard cutters of different types (i.e., flat and ball end-mills) and sizes should be selected for rough and finish milling. The main reasons for this are that the surface curvature often varies from one CC point to another and the open spaces for cutter at the CC points can be quite different. Consequently, using one cutter in the surface machining cannot be productive, and a group of appropriate cutters are necessary to keep a high material removing rate. With the basic model of an allowable cutter size for a CC point just proposed, the allowable sizes of the imaginary cutters can be

calculated for all the CC points. Theoretically, these imaginary cutters are perfect to cut the compound surface. However, these cutters are not standard and it is impractical to use the non-standard cutters because making an irregular cutter is very expensive. Therefore, a group of appropriate standard cutters have to be determined based on the calculated imaginary cutters.

An effective approach to selecting standard cutters is to compose a color map of standard cutter size; the color at each CC point indicates the largest standard cutter, which can be used to cut the CC point. Then a group of standard cutters can be properly selected according to the colors of the map. This map can be easily constructed in five steps: (1) listing all the standard cutters available in the company, (2) assigning different colors for these cutters, (3) computing the allowable cutter sizes at all the CC points, (4) at each CC point, comparing the allowable cutter size with the cutter list in order to find the largest standard cutter that is smaller than the allowable cutter size, and (5) plotting the corresponding color of the selected standard cutter at this CC point. Since the selected standard cutter is smaller than the allowable cutter at each CC point, the selected standard cutters can cut the compound surface without gouging and interference.

The main feature of the color map of standard cutter size is that it can clearly show which region(s) can be machined with an appropriate standard cutter. Thus, based on the map, the standard cutters that are able to access large area of the compound surface will be selected in order to use large tools as much as possible and the standard cutters being able to access the bottom of concave shape will be selected for finish machining. The

principle of selecting the cutter is that this group of standard cutters should consist the cutters which can machine a large region or can machine roots and bottoms of the compound surface. This group of appropriate standard cutters can machine the compound surface efficiently in roughing and produce the surface accurately in finishing.

4.3 3-Axis milling of a hair dryer mold

This innovative approach is effective and practical in determining appropriate standard cutters for 3-axis CNC milling of compound surface parts. To demonstrate its advantages, this approach has been applied to machine a hair dryer injection mold. In this example, the hair dryer mold is designed with the CATIA CAD/CAM software system (see Fig. 4-1 a). The compound surface of this mold includes 24 NURBS surface patches (see Fig. 4-1 b). These surface patches are connected with C^0, C^1 or C^2 continuity. The whole hair dryer surface has not only concave region but also convex region. It is very difficult or even impossible to determine which sizes of the cutters can machine these surfaces efficiently without gouging and interference.

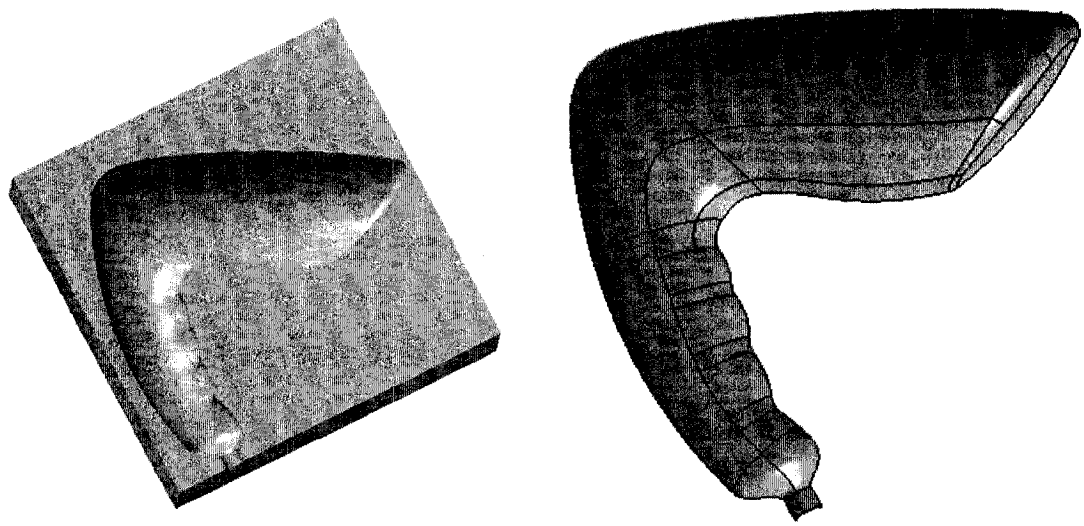

(a) (b)

Figure 4-1: (a) A hair dryer mold and (b) its 24 surface patches

To machine each surface patch, a mesh of 21×21 iso-parametric CC points is generated. The radii of the theoretical allowable flat and ball end-mills at each CC point can be calculated by using this proposed method. Suppose the standard flat end-mills are available in sizes of 25.4 mm (1 inch), 12.7 mm (1/2 inch), 6.35 mm (1/4 inch) and 3.175 mm (1/8 inch), and the ball end-mills are also available with the same sizes for the CNC machining. As we know, to machine a CC point, the allowable cutter is the largest cutter that can be used without gouging and interference, so the standard cutter for machining this point should be selected as large as possible but smaller than this theoretical allowable cutter. For machining all the CC points, the standard cutters available are

compared against the theoretical allowable cutter radii, and then several cutters can be chosen to cut the hair dryer surface patches in rough and finish machining. The results are shown in Fig. 4-2 and 4-3, in which the cutters are represented in different colors. In Fig. 4-2, the regions in dark brown can be cut in rough machining by using a flat end-mill with radius of 1 inch; the regions in light brown can be cut using a flat end-mill with radius of ½ inch; the green areas using a flat end-mill with ¼ inch radius; the light blue ares using a flat end-mill with $\frac{1}{8}$ inch radius; and the dark blue areas cannot be machined with the available cutters.

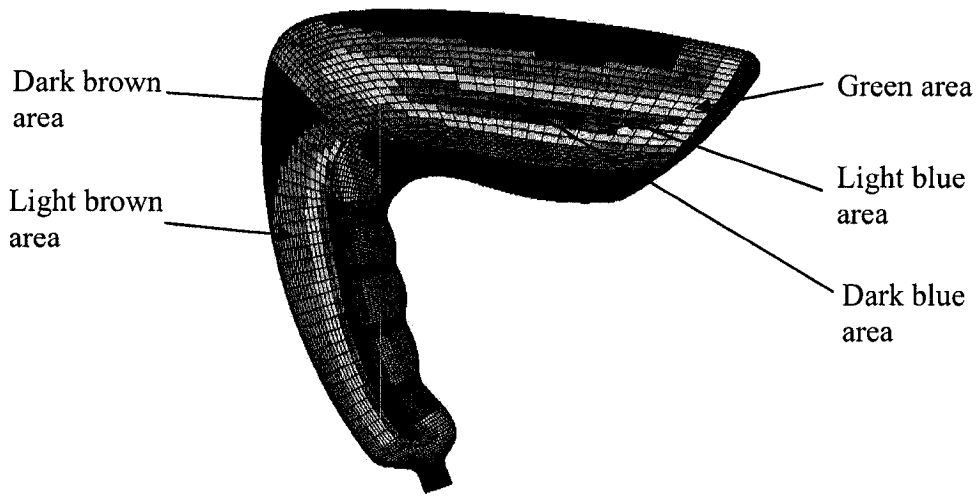

Figure 4-2: Standard cutter radii map for flat end-mills

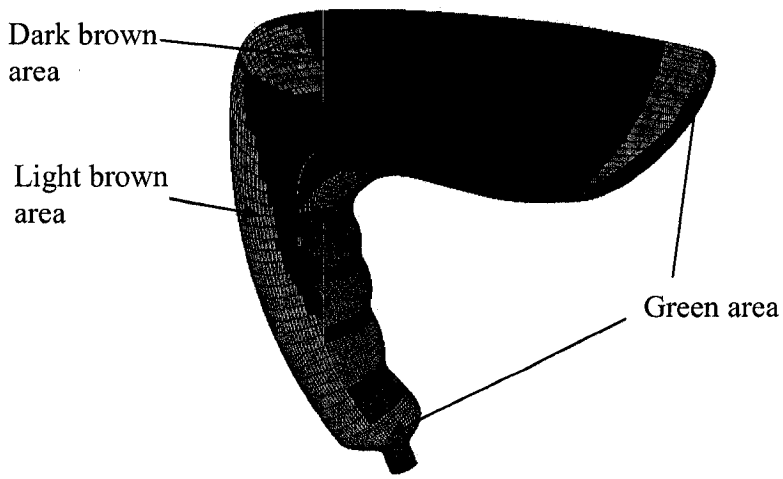

Figure 4-3: Standard cutter radii map for ball end-mills

4.4 Improved machining efficiency by using different cutters based on the allowable cutter sizes

In CATIA V5 R16, based on the standard cutter radii map for ball end-mill, we select 3 different sizes ball end-mills to perform the finish machining simulation of the hair dryer mold. Three cutters are: 2 inch, 1 inch and ½ inch diameter ball end-mills in sequence. Each cutter only machines an area where it can reach without gouging and interference. The areas machined by differenet cutters will not overlap with each other. The machining simulation result is shown in Fig. 4-4.

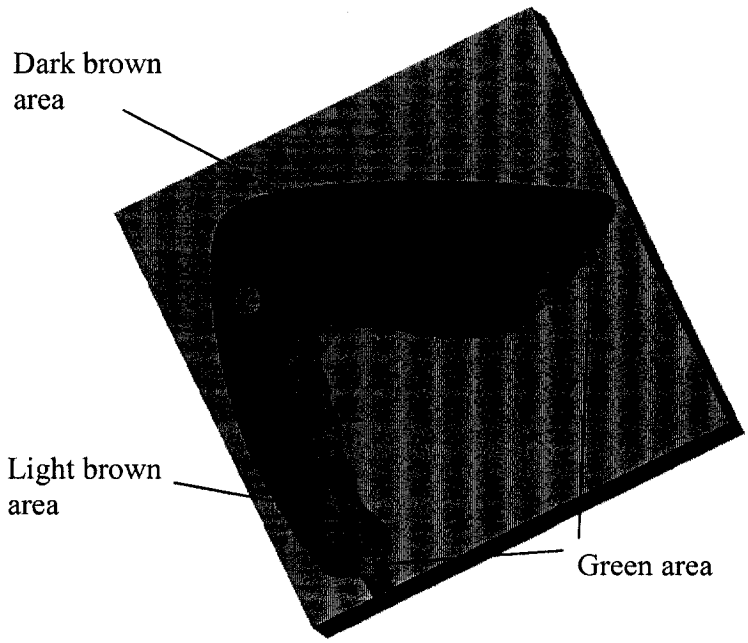

Figure 4-4: Machining simulation using 2 inch, 1inch and ½ inch ball end-mill for the hair dryer mold

Machining time and total time for different cutters are listed in Tab. 4-1. The dark brown area are formed by 2 inch diameter ball end-mill, light brown area by 1 inch diameter ball end-mill and green area by 1/2 inch diameter ball end-mill. Compared Fig. 4-4 with Fig. 4-3, our approach is proven in CATIA CAD/CAM system. It can be used for cutters selection before tool path planning, and this will contribute to a high machining efficiency by using different cutters. A test by using one 1/2 inch ball end-mill to

machine all 24 hair dryer surface patches was done. In this test, same tolerance and scallop height are set, the machining time and total time are also listed in Tab. 4-1.

Table 4-1: Machining time and total time using one or three ball end-mills to mill hair dryer mold.

Time (minute)	Three ball end-mills with different sizes				One cutter
	2 inch	1 inch	½ inch	Total	½ inch
Machining time	9.10	12.20	2.27	23.57	53.65
Total time	9.40	12.93	2.62	24.95	54.23

Through Tab. 4-1, the total machining time by using three ball end-mills (2 inch, 1 inch and 1/2 inch) is less than the half of the machining time by using one ball end-mill (1/2 inch). It shows that our method can greatly increase the machining efficiency.

Chapter 5 Application: 4-Axis CNC Milling of Gas Turbine

5.1 Introduction

As important components of gas turbine engines, axial-flow compressors are now designed with the advanced CAD techniques to improve their aerodynamic performance, and thereby increase the engines' efficiency. In particular, the pressure and suction sides of the airfoils (or blades) are modeled with non-uniform rational B-spline (NURBS) surfaces, so the airfoil designs are often complex in shape and are closely spaced. However, it is quite challenging to effectively produce axial-flow compressors with several airfoils and a hub as a single piece on 4-axis CNC machines. Technically, the major difficulty in CNC programming for the airfoil milling is to determine the optimum angle of cutter-orientation for machining each pre-determined cutter-contact (CC) point, so that the cutter will not gouge the surface and the cutter shank will not interfere with the neighbouring airfoils. Much research has been conducted to detect and prevent any cutter-part interference and gouging in 4- and 5-axis milling; unfortunately, an effective automated solution has not yet been found.

Among the published, relevant works, Suh and Lee [12-13] proposed an algorithm to deal with step- and cutter-size determination, and tool-axis interference in 4-axis milling of revolving free-form surfaces. This algorithm first simplified this 4-axis machining with a 2D model and then tried to calculate critical points for the feasible range of the tool axis. In 1998, they [14] suggested quasi 5-axis machining technique by using a 3-axis machine and an index table, and developed an approach to optimizing the number of part set-ups according to the part's geometric shape. Teramoto et al. [15] recently proposed a new method for 5-axis non-interference machining of centrifugal compressors; this method includes two steps: (1) the generation of a surface between two adjacent blades at the entrance of the pitch space based on each prescribed tool-path of CC points on the blades, and (2) the location of a tool-axis point on this surface for each CC point in order to determine an appropriate cutter-orientation. Also, Young and Chuang [17] tried a method of cutter orientation determination for 5-axis flank milling of centrifugal compressors. Youn et al. [16] conducted research into interference-free tool-paths for 5-axis machining of marine propellers. Through a vertical plane intersecting with the blades, the bounding vectors for collision-free space can be found on the plane to approximately determine a cutter-orientation for milling the corresponding CC point. All of these methods either could not consistently and accurately model the multi-axis CNC milling, or are too difficult to implement in commercial CAD/CAM software systems.

Besides the research on compressor and propeller manufacturing, many other approaches have been proposed to calculate cutter-orientations in 5-axis milling of sculptured surfaces. Chiou and Lee [18] optimized cutter orientations to prevent local,

side, and rear gouging on a single surface. Yoon et al. [6] set up a collision-free condition in 5-axis milling by approximating the cutter and part surfaces in the vicinity of a CC point with Taylor's quadratic equation. Later, Yoon [7] introduced a concept of machined region width in order to optimize cutter-orientations in 5-axis machining. Since his assumption that the approximation was accurate for a large neighbouring area around a CC point is not true, his work was impractical. Rao and Sarma [8] applied the curvature comparison technique to the nominal part and cutter-swept surfaces for detecting the local gouging when using flat end-mills in 5-axis machining. Wang and Yu [9] specified the cutter-orientation along the minimum curvature direction for wider machining strips and carried out rough inspection for gouging. Unfortunately, cutter-part interference has not been successfully addressed in any of these works, and they therefore cannot be used to solve the problem in our research.

The main source of failure during compressor blade making is cutting tool collision with the blades. In our work, a novel, practicable approach is proposed to automatically determine cutter-orientations for 4-axis gouging- and interference-free machining of the airfoils. The original idea includes (1) in one set-up (the rotary table is fixed at an angle), the size of an imaginary cutter can be uniquely determined according to a CC point on the airfoil to be machined, the airfoil normal at this point, and a testing point (that can be any point either on this airfoil or other neighbouring surfaces); (2) for all the testing points, incrementally smaller sizes of the imaginary cutters are tested for gouging and interference, until the first non-gouging, non-interference smallest among them (called the allowable cutter) is determined; this cutter is the largest cutter that can cut at this CC

point without interference and gouging; and (3) by turning the rotary table to different angles, a group of allowable cutters can be found, and the biggest one (called the largest allowable cutter) can be identified together with the corresponding angle of the table (the optimum cutter orientation). This new approach first establishes a mathematical model of testing cutter size in terms of the rotary table angle in 4-axis CNC milling. Then a global optimization method – the particle swarm optimization method – is applied to this model to calculate the biggest allowable cutter and the optimum cutter orientation for any CC point. This proposed approach can accurately and automatically calculate cutter orientations for a set of appropriate cutters without local gouging and global interference. Since it is efficient and reliable, it can be directly implemented in the CAD/CAM systems to benefit the manufacturing industry.

To efficiently machine the airfoils, a group of standard cutters with different sizes have to be used due to various open spaces for the cutters at different CC points. For example, to cut the top area of an airfoil, a bigger cutter can be used; while for the bottom, a smaller cutter has to be employed in order to avoid gouging and interference. In practice, tapered or un-tapered end-mills (e.g. flat, ball-nose, and bull-nose end-mills) are often used to make the blades.

5.2 Applications

To demonstrate its advantages in determining cutter-orientations automatically, this novel approach is applied to an axial-flow compressor for its 4-axis machining. This part

design is shown in Fig. 5-1, whose outside diameter is 288 *mm* and width is 90 *mm*. For the 12 blades of this part, their pressure and suction surfaces are designed with two NURBS surfaces, whose control polygon contains 6 by 6 control points and whose boundaries are prescribed NURBS curves. The parameters of the NURBS surfaces are specified as u and v, the degrees of the basis functions of u and v are 5, and all weights of the control points are 1. To cut the blades, a mesh of 41 by 41 CC points on the pressure and suction surfaces are planned, and any CC point is represented with a pair of u and v values. The cutter-orientation at each CC point should be found automatically.

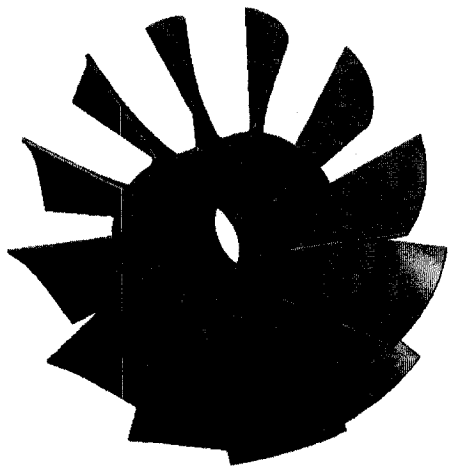

Figure 5-1: Example of an axial-flow compressor to be machined.

Our approach is applied to this example, and the cutter model is defined as a tapered bull-nose end-mill with corner radius r as 3 mm, taper angle θ as 5° and conical angle ψ as 0°. After calculation, the largest allowable size of the cutter and the corresponding cutter-orientation are found at every CC point; therefore, the graphs of the cutter size and cutter-orientation for the pressure and suction surfaces are plotted in Fig. 5-3 (a) (b) and Fig. 5-4 (a) (b), respectively. Since the biggest allowable cutter size at a CC point represents the maximum open space for cutter, the plot of largest allowable cutter sizes can be used as a reference to select appropriate cutters. Likewise, the plot of optimal angles of rotary table represents the cutter orientations for machining all the CC points.

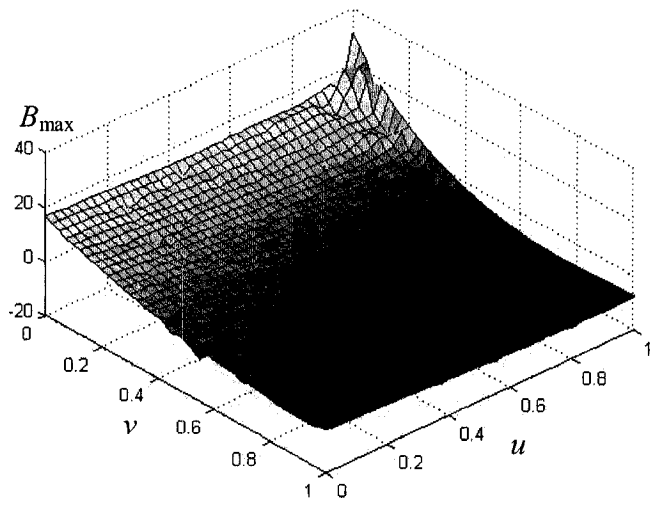

(a)

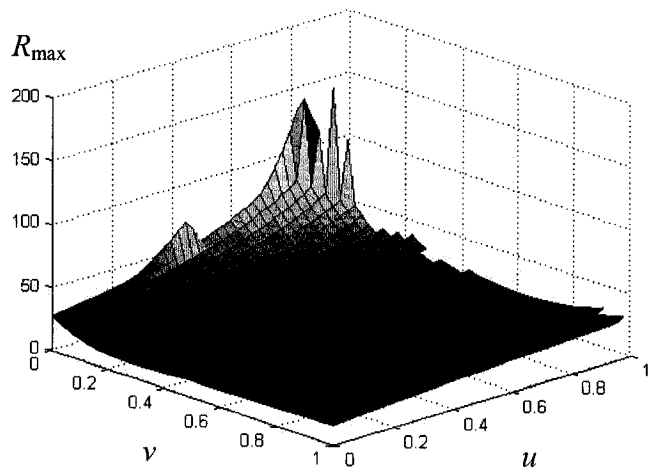

(b)

Figure 5-2: (a) The cutter-orientations, and (b) the maximum allowable cutter size for the specified CC points on the pressure surface

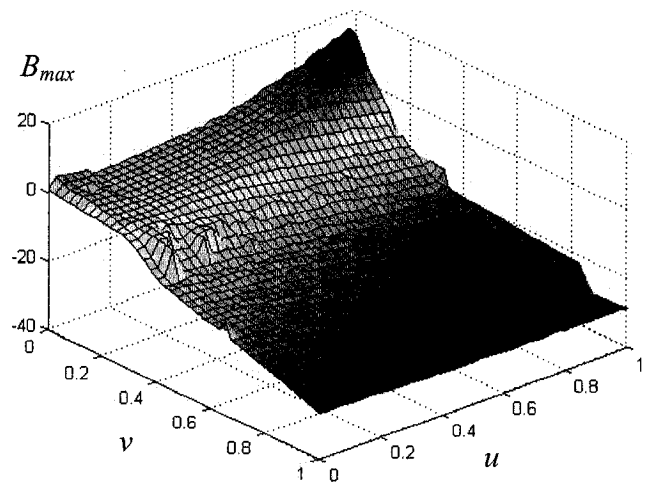

(a)

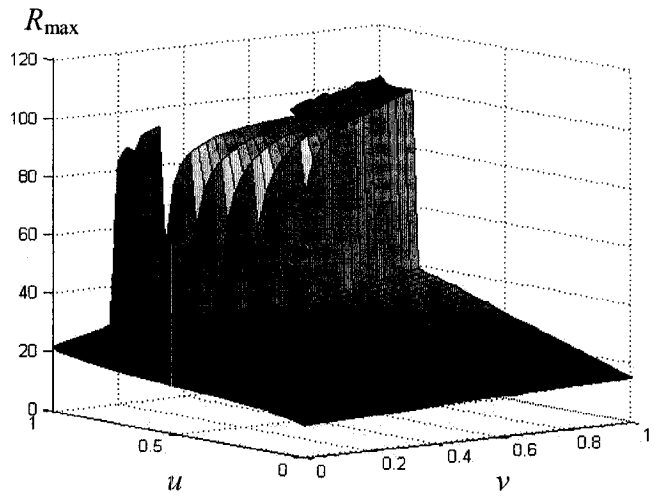

(b)

Figure 5-3: (a) The cutter-orientations, and (b) the maximum allowable cutter size for the specified CC points on the suction surface

In this work, a group of cutters available in the manufacturing company are selected and compared against the optimal cutter sizes of all CC points. The size of a cutter to be used to machine a CC point should be smaller or equal to that of the optimal cutter calculated; however, the cutter should be always as large as possible. The optimal cutter orientation at this CC point can be determined based on the plot of the angle of the rotary table. As a result, two tapered bull-nose end-mill with the diameter D as 19.05 *mm* (3/4 inch) & 38.1 mm (3/2 inch) and the tapered angle as 2° are selected in order to cut the airfoils without gouging and interference.

To verify this selected cutter, simulation of cutting the airfoils with this cutter on a 4-axis milling center is conducted with the CATIA V5R16 CAD/CAM system. The details

of the machined blade, the pressure surfaces and suction surfaces after simulation are shown in Fig. 5-5(a) (b) and (c) respectively. Airfoils are cut without gouging and interference, and high machining efficiency is achieved by using optimal cutters. Through this example, this approach demonstrates its advantage in the tool size and orientation determination in 4-axis surface milling, and can be easily implemented in CAD/CAM software in the manufacturing industry.

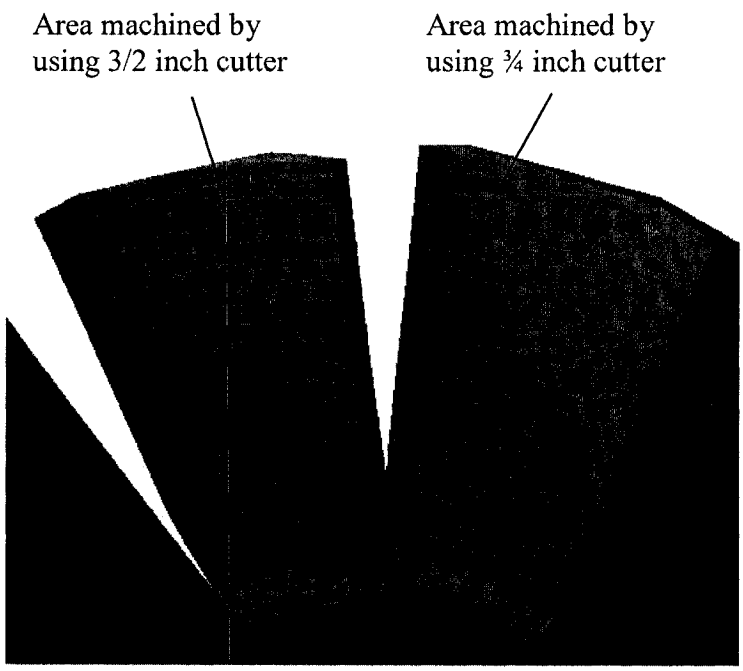

(a)

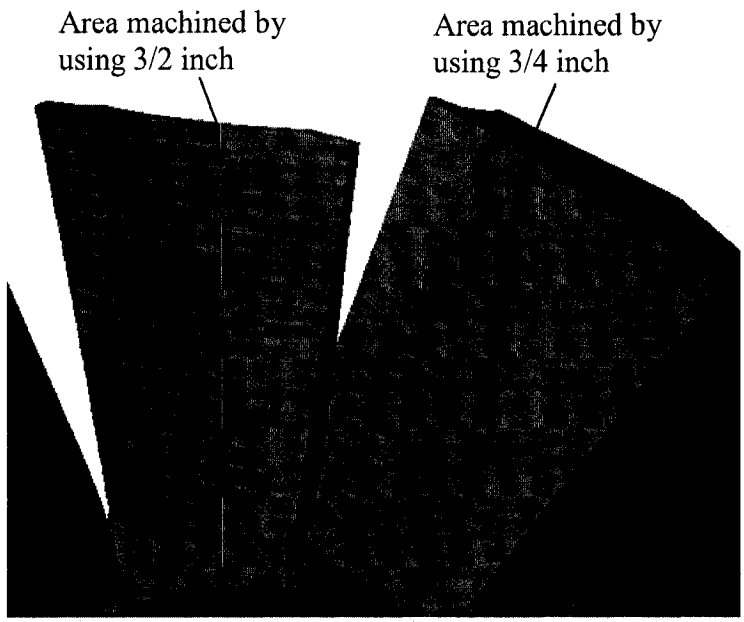

(b)

(c)

Figure 5-4: (a) The details of the pressure surface after the machining simulation, (b) the details of the suction surface after the machining simulation and (c) Machined blade in a simulation.

Chapter 6 Conclusions and Future Research

6.1 Conclusions

In this work, an innovative approach has been proposed to find the allowable cutter at every CC point in 3-axis sculptured surface milling. The major contributions include: (1) establishment of a mathematical model of optimal cutters, (2) derivation of the closed-form equations of imaginary cutter sizes, and (3) formulation of the allowable cutter size with a global optimization problem (the minimum one among all imaginary cutter sizes). By using this method, the allowable cutters at all the CC points on the sculptured surface can be found efficiently and accurately. For 3-axis sculptured surface machining, after calculating the allowable cutter sizes, an allowable cutter size map can be generated. Because the allowable cutter is the maximum cutter to machine the CC point without gouging and interference. Based on this map, a group of standard cutters can be selected to be as large as possible for high machining efficiency.

This proposed method has been extended to 4-axis CNC milling of free-form surfaces. Since the allowable cutter at a CC point varies in size with the change of cutter orientation, the maximum allowable cutter is represented with an optimization model, in which the variable cutter orientation (angle A, B or C) varies within the rotation limits of

the 4-axis milling machine. Thus, the maximum allowable cutter sizes and their corresponding orientations can be computed automatically. Based on the graphs of the maximum allowable cutter size and orientation, appropriate standard cutters can be selected and their orientations can be used in 4-axis milling in order to effectively eliminate gouging and interference and efficiently produce the sculptured parts.

Moreover, a hybrid optimization method is proposed in this work to synthesize the PSO and gradient optimization methods. By taking the advantages of these two methods, the hybrid method is able to search globally for the local region where the optimizer locates and can converge to the local optimizer quickly. Therefore, it is more effective in solving complex global optimization problems, compared to the conventional methods. In all, since this new approach to determining optimal cutter sizes and orientations is efficient and reliable, it can be directly implemented in the CAD/CAM systems to benefit the manufacturing industry.

6.2 Future research

The following topics are suggested for future work to expand the present research work:

- Cutter size and orientation determination in 5-axis CNC milling

Theoretically, our method can be applied in 5-axis CNC milling if inclination angle and tilt angle, instead of orientation angle, are used as variables in the objective function for the maximum allowable cutter size.

- Tool path verification in 5-axis CNC milling

Our approach can calculate the maximum cutter size without gouging and interference. So, for a given tool path which composes the sequent CC points and their orientations, we can apply our method to calculate the maximum cutter size at each CC point and intermediate positions between two sequent CC points. If a calculated cutter size at one point is less than the cutter size which we uses, that means gouging or interference occurs. The difference between the calculated cutter size and actual cutter size indicates the extent of gouging and interference. And then, over-cut can be calculated in terms of the cutting surface and sculptured surface at this CC point.

- Software development for cutter size selection in CAD/CAM system

Till now, we have not found a CAD/CAM software which can supply cutter size selection function before tool path planning. It is not convenient or even impossible for people to find the optimal cutter sizes to machine a sculptured surface efficiently. If our method can be integrated into CAD/CAM system, it will benefit the manufacturing industry to greatly increase the productivity.

Publication

Zezhong C. Chen, and Gang Liu, "Automated Tool-Orientation Determinations for 4-Axis Non-Gouge, Non-Interference Milling of Axial-Flow Compressors Airfoils" Proceedings of ASME Turbo Expo 2007 conference on Gas Turbine Technical Congress and Exposition, May 14-17, 2007, Montreal, Canada

Zezhong C. Chen, and Gang Liu, 2007, "An Automatic Approach to Multiple Cutters of Maximum Allowable Sizes for 3-Axis Milling of Compound Surface Parts," Submitted to Journal of Manufacturing Science and Engineering, ASME Transactions.

Zezhong C. Chen, and Gang Liu, 2007, "Automated Cutter-Orientation Determinations for 4-Axis Non-Gouging, Non-Interference Milling of Axial-Flow Compressors Airfoils," Submitted to Journal of Engineering for Gas Turbines and Power, ASME Transactions.

Bibliography

[1] Jensen, C.G. Red, W.E. and Pi, J., Tool selection for five-axis curvature matched machining, Computer-Aided Design, Vol. 34, 2002, pp 251-266.

[2] Glaeser, G. Wallner, J. and Pottmann, H., Collision-free 3-axis milling and selection of cutting tools, Computer-Aided Design, Vol. 31, 1999, pp 225-232.

[3] Lo, C.-C., Two-stage cutter-path scheduling for ball-end milling of concave and wall-bounded surfaces, Computer-Aided Design, Vol. 32, 2000, pp 597-603.

[4] Lee, Y.S. and Chang, T.C., Automatic cutter selection for 5-axis sculptured surface machining, International Journal of Production Research, Vol. 34, 1996, pp 997-998.

[5] Yang, D.-C.-H. and Han, Z., Interference detection and optimal tool selection in 3-axis NC machining of free-form surfaces, Computer-Aided Design, Vol. 31, No. 5, 1999, pp 371-377.

[6] Yoon, J.-H. Pottmann, H. and Lee, Y.-S., Locally optimal cutting positions for 5-axis sculptured surface machining, Computer-Aided Design, Vol. 35, 2003, pp 69-81.

[7] Yoon, J.-H., Tool tip gouging avoidance and optimal tool positioning for 5-axis sculptured surface machining, International Journal of Production Research, Vol. 41, No. 10, pp 2125-2142.

[8] Rao, A., and Sarma, R., On local gouging in five-axis sculptured surface machining using flat-end tools, Computer-Aided Design, Vol. 32, 2000, pp 409-420.

[9] Wang, X.-C., and Yu, Y., An approach to interference-free cutter position for five-axis free-form surface side finishing milling, Journal of Material Processing Technology, Vol. 123, 2002, pp 191-196.

[10] George, K.-K. and Babu, N.-R., On the effective tool path planning algorithms for sculptured surface manufacture, Computers and Industrial Engineering, Vol. 28, No. 4, 1995, pp 823-838.

[11] Hatna, A. and Grieve, R.-J., Pre-processing approach for cutter interference removal, International Journal of Production Research, Vol. 39, No. 3, 2001, pp 435-460.

[12] S.H. Suh, K.S. Lee, Avoiding tool interference in four-axis NC machining of rotationally free surfaces, IEEE Transactions on Robotics and Automation, 8 (6) (1992) 718-729.

[13] S.H. Suh, K.S. Lee, A prototype CAM system for four-axis NC machining of rotational-free-surfaces, Journal of Manufacturing Systems, Transactions of SME, 10 (4) 1991 322-331.

[14] S.H. Suh, J.J. Lee, Five-axis part machining with three-axis CNC machine and indexing table, Journal of Manufacturing Science and Engineering, Transactions of ASME, 120 (1998) 120-128.

[15] K. Teramoto, M. Morikawa, T. Ishida, Y. Takeuchi, Five-axis control tool-path generation using curved surface interpolation, Proceedings of the 2nd International

Conference on High Performance Cutting, June 12-13, 2006, Vancouver, BC, Canada.

[16] J.W. Youn, Y.T. Jun, S.Y. Park, Interference-free tool-path generation in five-axis machining of a marine propeller, International Journal of Production Research, 41 (18) (2003) 4383-4402.

[17] H.T. Young, L.C. Chuang, An integrated machining approach for a centrifugal impeller, International Journal of Advanced Manufacturing Technology, 21 (2003) 556-563.

[18] J.C.J. Chiou, Y.S. Lee, Optimal tool orientation for five-axis tool-end machining by swept envelope approach, Journal of Manufacturing Science and Engineering, Transactions of ASME, 127 (2005) 810-818.

[19] Oliver, J.-H. Wysocki, D.-A. and Goodman, E.-D., Gouge detection algorithm for sculptured surface NC generation, Journal of Engineering for Industry, Transaction of ASME, Vol. 115, 1993, pp 139-144.

[20] Yu, D. Deng, J. Duan, Z. and Liu, J., Generation of gouge-free cutter location paths on freeform surfaces for non-spherical cutters, Computers in Industry, 1996, Vol. 28, pp 81-94.

[21] Zhou, L., and Lin, Y.-J., An effective global gouge detection in tool-path planning for free-form surface machining, The International Journal of Advanced Manufacturing Technology, Vol. 18, 2001, pp 461-473.

[22] Tao Chen, Peiqing Ye, and Jinsong Wang, Local interference detection and avoidance in five-axis NC machining of sculptured surfaces, The International Journal of Advanced Manufacturing Technology, Vol. 25, 2005, pp 343-349.

[23] Yuan-Shin Lee, and Tien-Chien Chang, 2-Phase approach to global tool interference avoidance in 5-axis machining, Computer-Aided Design, Vol. 27, 1995, pp 715-729.

[24] J.-M. Redonnet, W. Rubio, F. Monies and G. Dessein, Optimising tool positioning for end-mill machining of free-form surfaces on 5-axis machines for both semi-finishing and finishing, The International Journal of Advanced Manufacturing Technology, Vol. 16, 2000, pp 383-391.

[25] Chen Wenliang, Zeng Jianjiang, Li Lei, and Ding Qiulin, An approach to gouging avoidance for sculptured surface machining, Journal of Materials Processing Technology, Vol. 138, 2003, pp 458-460.

[26] Joung-Hahn Yoon, Tool tip gouging avoidance and optimal tool positioning for 5-axis sculptured surface machining, International Journal of Production Research, Vol. 41, 2003, pp2125-2142.

[27] Suk-Hwan Suh, and Kee-Sang Lee, Avoiding tool interference in four-axis NC machining of rotationally free surfaces, IEEE Transactions on Robotics and Automation, Vol. 8, 1992, No. 6, pp 718-729.

[28] Paul J. Gray, Sanjeev Bedi, and Fathy Ismail, Arc-intersect method for 5-axis tool positioning, Computer-Aided Design, Vol. 37, 2005, pp 663-674.

[29] Byoung K. Choi, and Robert B. Jerard, 1998, Sculptured surface machining: theory and applications, Kluwer Academic Publishers.

[30] V. Kelner, et al., A hybrid optimization technique coupling an evolutionary and a local search algorithm, Journal of Computational and Applied Mathematics (2007), doi: 10.1016/j.cam.2006.03.048.

[31] Pigel L, Tiller W. The NURBS Book. 2nd ed., Berlin: Springer-Verlag, 1997. 81-138.